DESIGNING OF RADIATION SHIELDING COMPOSITES PREPARED FROM INDIGENOUS RAW MATERIALS

By

Mohammad Mahfujur Rahman

Master of Philosophy in Chemistry

Department of Chemistry

BANGLADESH UNIVERSITY OF ENGINEERING AND TECHNOLOGY (BUET),

DHAKA-1000

June, 2022

Bangladesh University of Engineering and Technology (BUET), Dhaka-1000
Department of Chemistry

Certification of Thesis

A thesis on

DESIGNING OF RADIATION SHIELDING COMPOSITES PREPARED FROM INDIGENOUS RAW MATERIALS

By

Mohammad Mahfujur Rahman

Roll No.: 0416033205, Session: April 2016, has been accepted as satisfactory for the degree of Master of Philosophy (M.Phil.) in Chemistry and certify that the student has demonstrated satisfactory knowledge of the field covered by this thesis in an oral examination held on 15 June, 2022.

BOARD OF EXAMINERS

1. **Dr. Md. Shakhawat Hossain Firoz**
   Professor
   Department of Chemistry
   BUET, Dhaka-1000

   Supervisor & Chairman

2. **Dr. Md. Abdur Rashid**
   Professor & Head
   Department of Chemistry
   BUET, Dhaka-1000

   Member (Ex-officio)

3. **Dr. Ayesha Sharmin**
   Associate Professor
   Department of Chemistry,
   BUET, Dhaka-1000

   Member

4. **Dr. Chanchal Kumar Roy**
   Assistant Professor
   Department of Chemistry,
   BUET, Dhaka-1000

   Member

5. **Dr. Md. Mufazzal Hossain**
   Professor
   Department of Chemistry
   University of Dhaka

   Member (External)

CANDIDATE'S DECLARATION

It is hereby declared that this thesis or any part of it has not been submitted elsewhere for the award of any degree or diploma.

Mohammad Mahfujur Rahman

DEDICATION

I dedicate this thesis to my beloved mother Mrs. Mahmuda Khanum (1955 to date).

Mrs. Mahmuda Khanum was a Senior Asst. Teacher (Rtd. in 2015) of Uthali Pilot Girls High School (EIIN Code 111040, MPO Number: 2806041302), Shibalaya, Manikgonj.

She had completed her B.A. degree from Dhaka Board in 1996 and B. Ed. Degree in 1999-200 session. She is a brilliant, polite and efficient woman I have ever seen.

I have been passing quality times with her that feels tremendous joy and happiness. May Allah bestow upon her by long, healthy and peaceful life.

Table of Contents

Page No.

CHAPTER 3

List of Figures

List of Tables

List of Abbreviations of Technical Symbols and Terms

1. *LAC (μ_L): Linear Attenuation Coefficient*
2. *MAC (μ_m):Mass Attenuation Coefficient*
3. *HVL: Half Value Layer*
4. *EDR: Effective Dose Rate*
5. *RBS: Raw Beach Sand*
6. *M: Magnetite*
7. *I: Ilmenite*
8. *IS: Inland Sand*
9. *RMI: Radiation Matter Interaction*
10. *ROI: Region of Interest*

Acknowledgement

At the very beginning, I humbly acknowledge my deepest gratitude to the almighty, the most gracious, benevolent and merciful creator for his infinite mercy bestowed on me in carrying out the research work presented in the dissertation. It is a great pleasure for me to acknowledge my deepest sense of gratitude, sincere, appreciation, heartfelt indebtedness, and solemn regards to my reverend teacher and supervisor Dr. Md. Shakhawat Hossain Firoz, Professor, Department of Chemistry, Bangladesh University of Engineering and Technology (BUET), for his kind supervision, indispensable guidance, valuable and constructive suggestions, liberal help, and continuous encouragement during the whole period. I am quite fortunate to be a part of his ambitious research team. I would like to convey my deepest gratitude to Dr. Md. Shamsuzzaman, Chief Scientific Officer (CSO) for hiskind co-operation, valuable suggestions, guidance, and help during the research period at Secondary Standard Dosimetry Laboratory (SSDL), Institute of Nuclear Science & Technology (INST) in Bangladesh Atomic Energy Commission (BAEC). I am thankful to all other respected teachers of the Department of Chemistry, BUET, for their time to time support. I am thankful toDr. Md. Mosharraf Hossain Bhuiyan (CSO), Ms. Tanjim Siddiqua (SSO), and Ms. Nourin Arobi (SO) for their valuable support & research co-operation at SSDL Laboratory, BAEC. I am also grateful to Dr. Mohammad Rajib (PGeo), Dr. Rahat Khan (PSO), Dr. Nazia Rahman (PSO), Mr. Ragib Absar Ramon (SO), and Mr. Md. Nabul Sardar (SO) for their research co-operation in BAEC. I am grateful to the authority of BUET. I am highly grateful to all members of the board of examiners for their valuable suggestions and appreciated comments. I am thankful to my dear colleagues and all the members of my Research Group for their friendly cooperation and lovely encouragement throughout my research period. I would also like to thank all of the officers and staff of the Department of Chemistry, BUET for their continuous help during my study period.Finally, I would like to express my heartfelt indebtedness and profound gratitude to my beloved mother, wife and two sons for their continuous inspiration and immeasurable sacrifices throughout my study.

June, 2022 Mohammad Mahfujur Rahman

ABSTRACT

The present study emphasizes to analyze the ionizing radiation shielding effectiveness of mono-energetic photon of X-rays (65 keV to164 keV) and relatively high energy ɣ-rays (^{137}Cs; 661.5 keV to^{60}Co; 1250 keV) for the determination of shielding design of radiation facilities. Composites were fabricated by indigenous low-cost materials such as raw beach sand (RBS) of Cox's Bazar, Magnetite-Ilmenite (MI), Inland Sand (IS), Dyeing Sludge (DS) as filler and Madupur clay as binder and base matrix. The X-ray and γ-ray attenuation efficacies of the prepared composites and ordinary concrete (OC) were characterized and assessed using broad beam transmission geometry, GM detector, and stated in terms of linear attenuation coefficients (LAC), mass attenuation coefficients (MAC), Half Value Layers (HVL) and Effective Dose Rates (EDR). The key elements of these prospective samples were measured to analyze the presence of heavy elements by Neutron Activation Analysis (NAA) method using the TRIGA Mark-II Research Reactor. The attenuation efficiencies were also explained with the help of the entire internal structural morphology of the composites by thermal neutron radiography technique. The LAC values of MI composite and RBS composite decrease from 1.6443cm^{-1} to 0.1459cm^{-1} and 1.4026cm^{-1} to 0.1377cm^{-1}for 65 keV to 1250 keV respectively, which reveals the higher level of attenuation among the studied composites. The LAC data of ordinary concrete has exhibited a moderate level of attenuation (0.7189 cm^{-1}to 0.1314 cm^{-1} for 65 keV to 1250 keV). The IS and DS composite showed the poor attenuation capacity, the LAC falls down from 0.5150 cm^{-1} to 0.0974 cm^{-1} and 0.5133 cm^{-1}0.0949 cm^{-1}for 65 keV to 1250 keV, respectively. The MAC & EDR data with the increasing photon energy follows a similar pattern as LAC data. The sequences of HVL of the composites are MI<RBS<OC<IS. The morphology study reveals that the finely structured clay-based MI and RBS composites have lower gray values at various pixel points. The current experimental observations would be useful for designing potential radiation shielding materials at radiation facilities based on the indigenous cost-effective raw materials.

Key-words: *Linear attenuation coefficient (LAC), mass attenuation coefficient (MAC), half value layer (HVL), photon energy, raw beach sand, minerals, Madhupur clay etc.*

CHAPTER 1

1. INTRODUCTION

1.1 Ionizing Radiation and Their Sources

In the modern technological age, the ionizing radiations (X-rays, Gamma-rays etc.) as well as radioactive substances may be of natural or artificial origin which have numerous beneficial uses in medical treatment (nuclear medicine, radiology, radiotherapy etc.), industries, agriculture, radio-isotope production facility, nuclear power plant etc. (Figure-1). In a radiation facility the radiation occupational-workers, public and the surrounding environments are potentially become exposed to these radiations deliberately or accidentally [1].

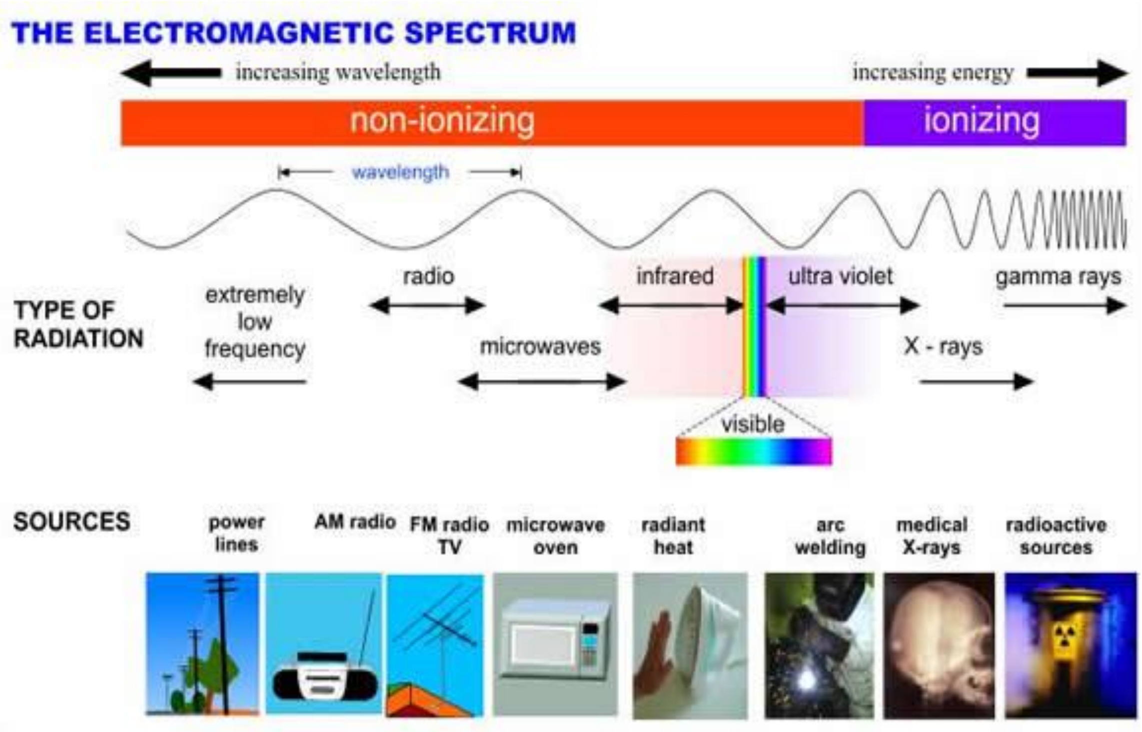

Figure-1.1: Types of radiation and their sources.

Ref: https://www.arpansa.gov.au/understanding-radiation/what-is-radiation (on 20.11.2021)

1.2 The Generation of X-ray

The X-ray investigation uses X-rays generated in X-ray tubes. A high voltage is applied between a cathode and an anode (tungsten, molybdenum, copper, etc.) inside an X-ray tube so that thermal electrons migrate from the cathode to the anode in a vacuum at high speed [2]. X-rays are generated when the direction of propagation of the thermal electrons changes as they are attracted to the nucleus of the anode are called braking X-rays. When an electron is ejected from the inner electron orbit of the anode nucleus, another electron migrates (transitions) to this vacancy from the outer electron orbit. X-rays generated thereby are called characteristic X-rays. Most of the X-rays generated in X-ray tubes are braking X-rays (Figure-1.2). Generation of X-rays stops when the X-ray tube is switched off.

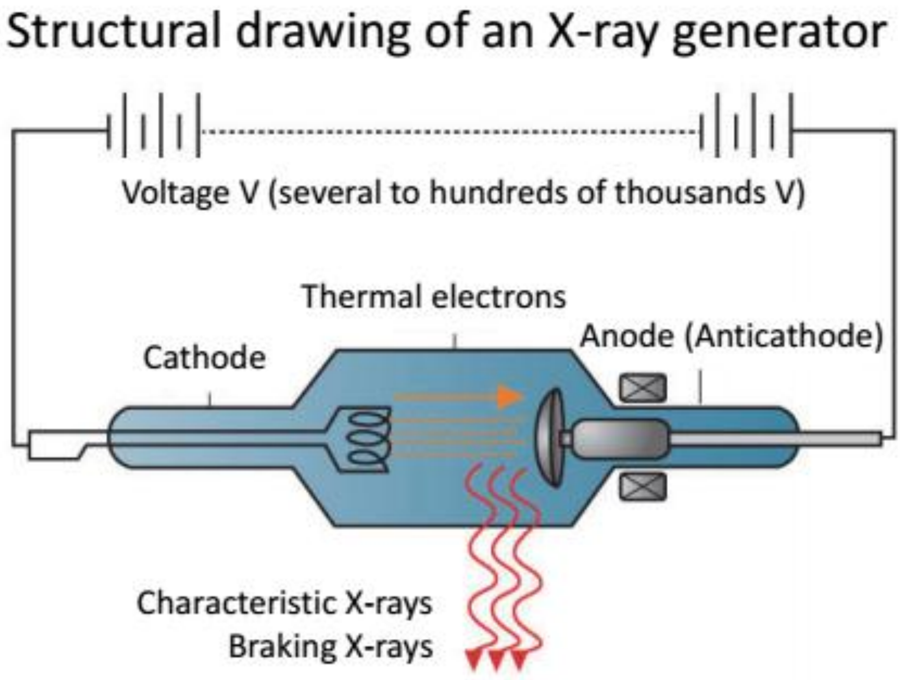

Figure-1.2: The X-ray generation by high voltage applying.

Ref: https://www.env.go.jp/en/chemi/rhm/basic-info/1st/01-03-04.html (on 21.11.2021)

1.3 The Emission of γ-ray

By following the nuclear phenomena, γ-ray (which is the high-energy electromagnetic radiation) is emitted from the nucleus of an atom which has a high penetrating ability. The nucleus with higher energy drops to lower energy level by emitting the γ-rays.The nucleus with spontaneous decay is the source of γ-rays (Figure-1.3).The γ-ray emission does not comprise a nuclear-transmutation reaction. The atomic number (Z) and the mass number (A) of a nucleus do not change through a γ-ray emission route.

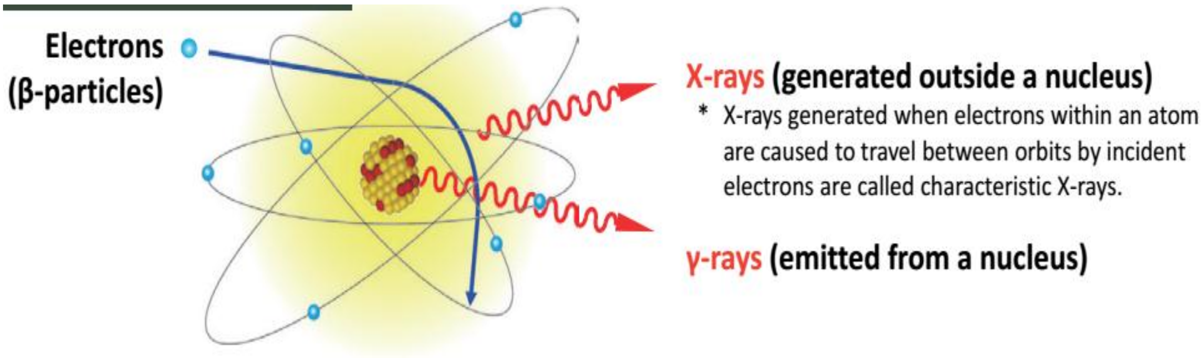

Figure-1.3: The X-rays generation and γ-rays emission.

Ref: https://www.env.go.jp/en/chemi/rhm/basic-info/1st/01-03-04.html (on 21.11.2021)

1.4 Radiation Effects on Biological System

Ionizing radiation poses significant hazards to living organisms. Itinteracts at the cellular level by following the steps of ionization, chemical changes and biological effect (Figure-1.4).

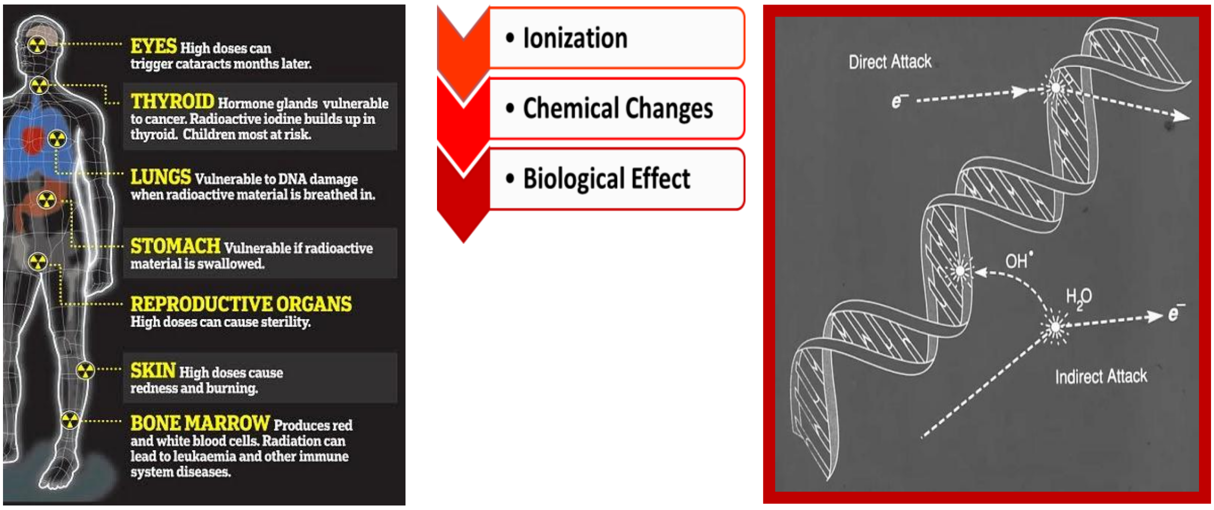

Figure-1.4: Radiation exposure to human body and interaction of ionizing radiation at cellular level.

Ref: https://fukushimahealtheffects.wordpress.com/health_and_radiation/ (on 21.11.2021)

The Exposure of tissues or organs to ionizing radiation can induce the death of cells on a measure that can be extensive enough to damage the function of the exposed tissue or organ. Effects of these types, which are called ‘deterministic effect’, are clinically noticeable in an individual only if the radiation dose exceeds a certain threshold. Above this threshold dose, a deterministic effect is more severe for a higher dose. However, there is a possibility that the non-lethal transformation of a cell could lead, after a latency period, to cancer in the individual exposed, if it is a somatic cell; or may lead to hereditary effects, if it is a germ cell. Such effects are called ‘stochastic’ effects (Figure-1.5).

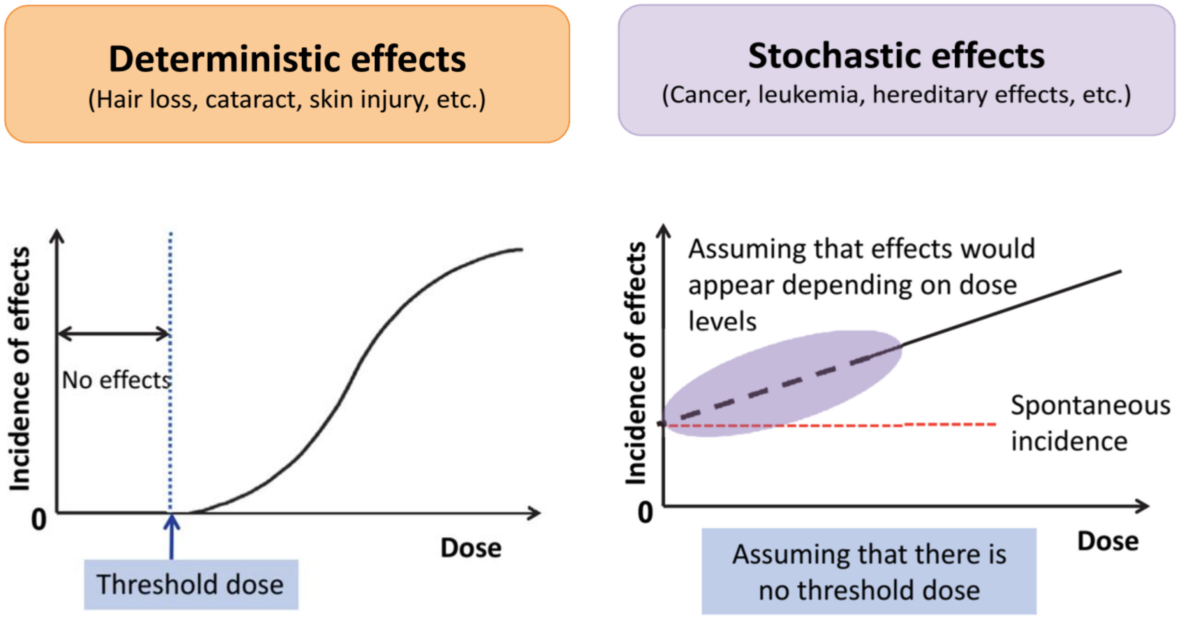

Figure-1.5: Effects of ionizing radiation in human body (deterministic and stochastic effects).

Ref: https://www.env.go.jp/en/chemi/rhm/basic-info/1st/03-01-04.html (25.11.2021)

1.5 Ionizing Radiation Exposure Guidelines

The radiation risks to the occupational-worker, people and the environment that may arise from the use of radiation and radioactive substance must be evaluated and controlled through the application of standards of safety.It has been recommended that the use of ionizing radiation (X-rays, Gamma-rays etc.) should be such that the radiation doses to occupational-workers, public and patients are As Low As Reasonably Achievable (ALARA) considering time, distance and shielding according to International Atomic Energy Agency (IAEA) guidelines [1]. To optimize this threat, radiation shielding can play a key role in to confirm a safe working environment (Figure-1.6). Therefore, sufficient and effective shielding is a prerequisite for the installation of such nuclear and radiation facilities to keep the radiation exposure below the dose limits recommended by the International Commission on Radiological Protection (ICRP) [3].

❖ **Justification**

✓ Benefit > Risk

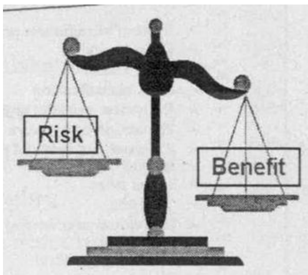

❖ **Optimization**

✓ IAEA ALARA Principle

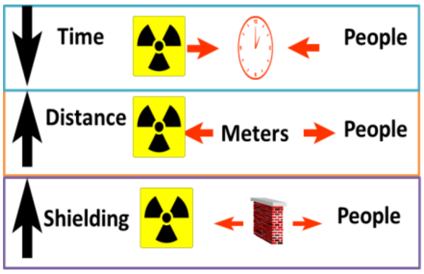

❖ **Dose Limit**:

✓ 20 mSv/Year (Occupational Worker)

✓ 1 mSv/Year (Public)

Figure-1.6: IAEA safety principles (Justification, Optimization and Dose Limit) and ICRP recomendation.

1.6 Effective Radiation Doses in Radiology

Depending on the type of radiological study performed, the patient characteristics and type of equipment, a wide variety of effective radiation doses [4] are executed (Table-1).

Table-1: Effective Radiation Doses of Common Radiological Procedures in Adults

	Radiation Dose* (mSv)	Chest X-Ray Equivalents	Comparable Lifetime Exposure Time to Natural Radiation
Chest x-ray	0.1	1	10 days
Abdominal x-ray	1	10	4 months
CT head	2	20	8 months
CT chest	7	70	2 years
CT abdomen or pelvis	10	100	3.3 years
PET/CT	5-20	50-200	20 months-6.7 years
Interventional cerebral angiogram	7-10	70-100	2-3.3 years
Coronary angiography	5-15	50-150	20 months-5 years

CT: computed tomography, PET: positron emission tomography. *Approximate effective dose.

The value of effective radiation dose for chest X-ray is 0.1 mSv (100 µSv), while the values are being maximized for PET/CT and angiography. But the frequencies of the chest X-ray investigation are usually higher than others. In order to make a generalized comparison, the values of chest X-ray equivalents and comparable lifetime exposure time to the natural radiation are also shown in table-1.

1.7 Penetration Power of γ-Ray and X-Ray

The γ-rays and X-rays have high penetrating power and travel several tens to hundreds of meters in the air. By colliding with the human body, they can reach deep into the body or sometimes pass through it. Their energy is imparted to the part they pass through [2]. In X-ray examination, the parts of the body X-rays can easily pass through (lungs, etc.) appear in black while the parts they cannot easily pass through (bones, etc.) appear in white. The γ-ray and X-ray consist of high-energy waves that can travel great distances at the speed of light and generally have a great ability to penetrate other materials (Figure-1.8). In spite of their capacity to penetrate other substances, in general, neither gamma-rays nor X-rays have the ability to create anything radioactive. Quite a few feet of ordinary-concrete or a few inches of dense material (such as lead, bismuth) are able to attenuate these types of ionizing radiation.

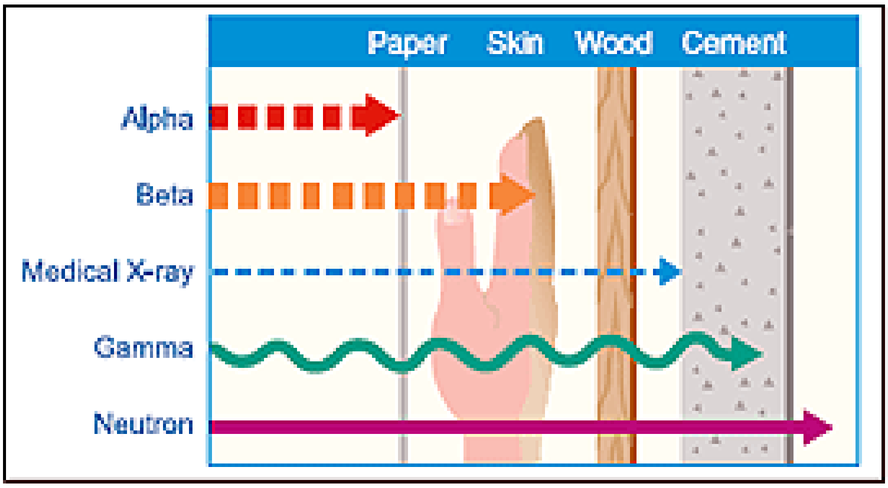

Figure-1.7: Penetration power of various forms of ionizing radiation.

https://www.nrc.gov/about-nrc/radiation/health-effects/radiation-basics.html (on 30.11.2021)

1.8 Designing & Fabrication of Radiation Shielding Materials From Indegenous Raw Sources

Conventionally, the thick ordinary concreteis being used as a radiation shielding wall to protect the radiation occupational workers, patients andthe public from radiation.In PET-CT facility the patient itself continuously emits high energy annihilation photon radiation during the whole procedure. In INMP facility, Bangladesh, all shielding walls and ceilings are made of concrete with a practical thickness of 30.48 cm (density 2.35g.cm^{-3}) for more safety [5]. Ordinary concretestresses a huge load onto the building structure and consumes more spaces at the radiation facilities.

In recent years, several relevant studies of the radiation shielding properties in terms of the linear and mass attenuation coefficients (LAC, MAC) for different building materials [6-7] consist of various matrixes, fillers and additives have been carried out. Most of these shields are made from different types of concretes, such as ordinary-concrete, heavy concrete (e.g., magnetite, Ilmenite,barite, steel, goethite, perlite etc.).

Concrete (for ceiling material) and bricks with two layers of cement (for the walls) are quite similar in the effectiveness of shielding for photons ranging from 50 keV to 3000 keV. The shielding effectiveness of bricks with no cement layer drops by about 40–50% for energies higher than 300 keV when compared to bricks covered on both sides [8-10].

Minerals and some other dense ingredients incorporated materials exhibit better radiation attenuations [11-14]. The neutron shielding properties of Ilmenite-magnetite (I-M) concrete was measured experimentally. The instantaneous relaxation length and thickness-dependent removal cross section of neutrons from a ^{252}Cf source penetrating I-M concrete with and without a cadmium sheet reported which indicated a good shielding effectives for nuclear reactor [15].

The promising results revealed the suitability of using concrete with added natural perlite mineral in the aggregate to shield low-energy gamma radiation as it has the lowest half value layer (HVL) [16]. High-performance heavy density concrete made with the fine portions of magnetite aggregate improves the shielding efficacy against gamma-rays for ^{137}Cs at photon energy of 0.662 MeV and ^{60}Co at photon energies of 1.173 and 1.333 MeV. Also, concrete made with magnetite fine aggregate has higher physico-mechanical properties than those containing barite and goethite [17].

The reinforced polymer composite materials with heavy minerals also presented relatively decent radiation shielding ability in comparison to the ordinary concrete-block [18-19]. The addition of hematite and chalcocite has been enhanced the mass attenuation coefficient (μ_m) of PVC polymers. It was also found that the μ_m of chalcocite/PVC is higher than that of hematite/PVC due to the copper content in the former [20].

Beach sand was found to be the best sand type for making concrete for ionizing radiation shielding in the diagnostic energy range of 60–1333 keV [21]. Clay is a naturally occurring material composed of fine grain minerals, which shows plasticity when moist and becomes hard when dried or fired. Clay has been used in the manufacturing of bricks since ancient times. The clay soils have better photon energy absorption characteristics than other soils [22-24]. Diverse soil and clay from different sites exhibit variable attenuation behavior. Sandy loam and sandy clay loam soils demonstrated poor photon energy absorption characteristics. However, clay loam and clay soils had good photon energy absorption characteristics [25-27].

Several other oxides like bismuth oxide (Bi_2O_3), lead oxide etc. have also been used as additives along with the fillers and matrix. Among them, the non-toxic but expensive bismuth oxide has a higher radiation attenuation property [28-29].

Theelemental compositional study reveals that inland sands contain low concentrations of the studied elements (Ce, Hf, Fe, Sb, Tb, Sc, Ta, Zn, Cs, Co and Eu) than those of beach sands [30].The given SEM images represent the presence of particles of varying morphology in the types of developed, non-toxic perlite mineral in radiation shielding concretes. The Microstructure of concrete shield was also considered [16, 31, and 32].

However, it is necessary to look for low-cost, eco-friendly and locally available innovative alternative shielding material for the rapid expansion of the nuclear industries and the extensive applications of radioactive substances in Bangladesh. To the best of our knowledge, very few studies have been carried out related to radiation parameters of clay (as a binder ingredient) based indigenous high dense components of beach minerals(magnetite,Ilmenite), raw beach sand (RBS), inland sand (IS), dyeing sludge (DS) etc. in different parts of the country. The literature survey reveals that clay has better photon energy absorption characteristic as compared to other types of soil.The composite of clay with different sand (RBS and IS), minerals and some additives could be a good alternative to the traditional shielding materials.

The present work is conducted by using Madhupur clay as a binder/matrix. It was strongly believed that the Madhupur tract represents tectonically uplifted surface of the

Pleistocene period [31]. Madhupur tract is considered as the Pleistocene Terraces (*Morgan & McIntire, 1959*). These are characterized by plateau like hillocks and the height varying from 9 to 18.5m but some peaks of Lalmai hills rise up to 40 meters or more. The sediments of the tracts are deeply weathered and strongly oxidized (brown reddish colored) and it is called Madhupur Clay (*Morgan & McIntire, 1959*).Fabrication of the indigenous composites containing fine-grained matrix of clay and cement with the filler of raw beach sand, beach minerals (magnetite, ilmenite), inland sand (ordinary building sand), dyeing sludge and additives like bismuth oxide (Bi_2O_3) and study of the attenuation of ionizing radiation of X-ray (photon energy range of 65 keV to 164 keV) and γ-ray of ^{60}Co and ^{137}Cs (photon energy range of 661.6 keV to 1250 keV)with the elemental composition, density, matrix thickness would play an important role to identify the proper shielding materials. Elemental abundance of the prospective materials was performed by neutron activation analysis (NAA) to identify the heavy elements and their impacts on radiation–matter interactions. The SEM images can exhibit the surface information of Nano/micro meter depth while the current morphological study by Neutron Imaging has shown and explained the entire internal structure and arrangement of several centimeters, because of neutron penetration efficacy.

1.9 Objectives

The main objectives of this present work are to

i. Design and fabricateand the indigenous radiation shielding composites utilizing clay and cement as the base matrix and raw beach sand, beach minerals (Magnetite, Ilmenite), dyeing sludge as fillers as well as bismuth oxide as additive.

ii. Determine the chemical composition (the key elements of the prospective shielding materials) by the Neutron Activation Analysis (NAA) using the 3MW TRIGA MARK-II Research Reactor.

iii. Determine the radiation attenuation capacity (in terms of Linear and Mass Attenuation Coefficient) and the shielding factor in terms of effective dose rates and Half Value Layer (HVL) of the prepared composites in the energy range of 65 - 164keV for X-rays and 662 - 1250 keV for gamma rays

iv. Analyze the mechanical (such as tensile strength, bending strength) and physical properties, such as, structural morphology (crack/hole detection), moisture desorption of the materials.

References:

[1] R.Abu-Eid, B. Ahier, "Radiation Protection and Safety of Radiation Sources: International Basic Safety Standards for protecting people and the environment", *IAEA Safety Standards, IAEA* - GSR Part 3, pp. 1-2, 2011.

[2]"BOOKLET to Provide Basic Information Regarding Health Effects of Radiation, Basic Knowledge and Health Effects of Radiation", Radiation Health Management Division, Ministry of the Environment, Government of Japan, Vol.1, pp. 13-27, 2019.

[3] R. M. Alexakhin, C. Cousins, A. J. Gonza ´ lez, Argentina H. Menzel, R. J. Pentreath, N. Shandala, B. C. Winkler, J. D. Boice Jr., R. Cox, L.-E. Holm, F.A. Mettler Jr., R.J. Preston, C. Streffer, J. Valentin, R.H. Clarke, G.J. Dicus, J.-K. Lee, Z.Q. Pan, Y. Sasaki, A. Sugier, P. Burns and J. Cooper, "ICRP - International Commission on Radiological Protection",*ICRP Publication 103, ELSEVIER*; *Vol.*103, pp.1-7, 2007.

[4] E. C.Lin, "Radiation risk from medical imaging", Mayo Clin Proc.(doi:10.4065/mcp.2010.0260); Vol. 85(12), pp.1142-1146, 2010.

[5] M. F. Uddin, R. Khatun, S. Akter, H. M. Jamil, A. N. Monika, M. A. Rahaman, R. P. Das, R. A. Sharmin, M. M. Rahman, M. M. Ahasan, "Radiation Shielding Analysis and Design of tof PET-CT Facility at Institute of Nuclear Medical Physics under Bangladesh Atomic Energy Commission, Bangladesh", *Int. J. Medical Physics, Clinical Engineering and Radiation Oncology,* Vol.8, pp.1-8, 2019.

[6] A. H. Taqi, H. J. Khalil; "Experimental and Theoretical Investigation of Gamma Attenuation of Building Materials";Journal of Nuclear and Particle Physics, Vol.7(1), pp.6-13, 2017.

[7] K.S. Mann, B. Kaur, G.S. Sidhu, A. Kumar, "Investigations of some building materials for ɣ-rays shielding effectiveness", Radiat. Phys. Chem. Vol.87, pp.16-25, 2013.

[8] I. C. P. Salinas, C. C. Conti, R. T. Lopes, “Effective density and mass attenuation coefficient forbuilding material in Brazil”, *Applied Radiation and Isotopes, ELSEVIER,*Vol. 64, pp.13–18, 2006.

[9] M. E. Medhat, “Gamma-ray attenuation coefficients of some building materials available in Egypt”,*Ann. Nucl. Energy,* (ELSEVIER)36, 849-852, 2009.

[10] I. Akkurt, H. Akyildirim, “Radiation transmission of concrete including pumice for 662, 1173, and 1332 keV gamma rays”, Nucl. Eng. Des., Vol.252, pp.163-166, 2012.

[11] M. Hossain Sahadath, R.Biswas, M. F. HUQ and A. S. Mollah,“Calculation of gamma-ray attenuation parameters for locally developed ilmenite-magnetite concrete”J. Bangladesh Acad. Sci., Vol. 40, No. 1, pp.11-21, 2016.

[12] C. Ipbuker, H. Nulk, V. Gulik, A. Biland, A.H. Tkaczyk, “Radiation shielding properties of novel cement-basalt mixture for nuclear energy applications”, Nucl. Eng. Des., Vol.284 pp.27-37, 2015.

[13] F. Budak Demir, G. Sahin, R. Karabulut, A. Oltulu, M. Un. A. “Determination of radiation attenuation coefficients of heavy-weight and normal-weight concretes containing colemanite and barite for 0.663 MeV γ-rays”. Annals of Nuclear Energy, 38, 1274-1278, 2011.

[14] I. Turkmen, Y. Ozdemir, M. Kurudirek, F. Demir, O. Simsek, R. Demirboga, “Calculation of radiation attenuation coefficients in Portland cements mixed with silica fume, blast furnace slag and natural zeolite”, Ann. Nucl. Energy, Vol.35, pp.1937-1943, 2008.

[15]S. I. Bhuiyan,F. U. Ahmed,A. S. Mollah &M. A. Rahman, “Studies of neutron shielding properties of ilmenite-magnetite concrete using a 252Cf source”, *Nuclear Technology*, Vol.93, pp.357-361, 1998.

[16] Osman Agara, Hüseyin O. Tekinb, M.I. Sayyedc, Mehmet E. Korkmaza, Ozgur Culfaa, Can Ertugayd, “Experimental investigation of photon attenuation behaviors for concretes including natural perlite mineral”, *Results in Physics , ELSEVIER*; Vol.12, pp.237–243, 2019.

[17] Ahmed S. Ouda, "Development of high-performance heavy density concrete using different aggregates for gamma-ray shielding", *HBRC Journal, Production and Hosting by ELSEVIER,* Vol.11, pp.328–338, 2015.

[18] M. M. Haque, M. Shamsuzzaman, M. B. Uddin, A. Z. M. Salahuddin, Ruhul A. Khan; "Fabrication and Characterization of Shielding Properties of Heavy Mineral Reinforced Polymer Composite Materials for Radiation Protection"; *EJERS, European Journal of Engineering Research and Science;* Vol. 4, No. 3, March 2019.

[19] K. S. Mann, A. Rani, M. S. Heer, "Shielding behaviors of some polymer and plastic materials for gamma-rays", Radiat. Phys. Chem., Vol.106, pp.247-254, 2015.

[20] K. A. Mahmoud, E. Lacomme, M. I. Sayyed, O. F. Ozpolat, O. L. Tashlykov, "Investigation of the gamma ray shielding properties for polyvinyl chloride reinforced with chalcocite and hematite minerals", *Heliyon*, Vol.6, pp.1-8, 2020.

[21] Folorunso O. Ogundare, "Low-energy broad-beam photon shielding data for constituents of concrete"; *Journal oF Applied Clinical Medical Physics*, Vol. 13 (Number 2), pp. 176-182, 2012

[22] Harjinder Singh Mann, Gurdarshan Singh Brar, Kulwinder Singh Mann and Gurmel Singh Mudahar, "Experimental Investigation of Clay Fly Ash Bricks for Gamma-Ray Shielding", *Nuclear Engineering and Technology*, Vol.48, pp.1230-1236, 2016.

[23] S. F. Olukotun, S.T. Gbenu, F.I. Ibitoye, O. F. Oladejo, H. O. Shittu, M. K. Fasasi, F. A. Balogun, "Investigation of gamma radiation shielding capability of two clay materials",*Nuclear Engineering and Technology,*Vol.50, pp.957-962, 2018.

[24] M. N. Alam, M. M. H. Miah, M. I. Chowdhury, M. Kamal, S. Ghose, R. Rumi, "Attenuation coefficients of soils and some building materials of Bangladesh in the energy range 276-1332 keV",*Appl. Radiat. Isot*., Vol. 54, pp. 973-976, 2001.

[25] Nil Kucuk, Zeynal Tumsavas and Merve Cakir, "Determining photon energy absorption parameters for different soil samples", *Journal of Radiation Research,* Vol.54, pp.578–586, 2013.

[26] Vishwanath P Singh, N. M. Badiger & Nil Kcuk, “Gamma ray and neutron shielding properties of some soil samples”, *Indian Journal of Pure and Applied Physics*, Vol.52, pp.579-587, 2014.

[27] F. Akmana, V. Turanc, M. I. Sayyed, F. Akdemire, M. R. Kaçal, R. Durakg, M. H. M. Zaidi, “Comprehensive study on evaluation of shielding parameters of selected soils by gamma and X-rays transmission in the range 13.94–88.04 keV using WinXCom and FFAST programs”,*Results in Physics*, *ELSEVIER*, 15 (2019) 102751

[28] J. P. McCaffrey, F. Tessier, and H. Shen, “Radiation shielding materials and radiation scatter effects for interventional radiology (IR) physicians”, *Am. Assoc. Phys. Med*., Vol.39 (7), pp.4537-4546, 2012.

[29] Mridula Dogra, K.J. Singh, Kulwinder Kaur, Vikas Anand, Parminder Kaur, “Gamma Ray Shielding and Structural Properties of Bi2O3-B2O3-Na2WO4 Glass System” *Universal Journal of Physics and Application*, Vol.11(5): pp.190-195, 2017

[30] M. A. Islam, S. Mahmud, S. M. Hossain, Sk. A. Latif, M. H. Ahsan,“Elemental Analysis of Raw Materials of Nuclear Reactor Shielding to Develop Low Activation Concrete”,*Journal of Nuclear Sciences*, Vol. 3, No.1(ISSN: 2148-7736), pp. 7-14, 2016.

[31] A. M. Brandt, D. J. Niedźwiedzka, “The influence of ionizing radiation on microstructure and properties of concrete shields – a review”. Cement Wapno Beton, 4, 216 – 237, 2013.

[32] Towhida Rashid, Md. Hossain Monsur and Shigeyuki Suzuki, “A Review on the Quaternary Characteristics of Pleistocene Tracts of Bangladesh”, *Earth Science Reports*, *OKAYAMA University, Japan*, Vol. 13, No. 1, pp.1-13, 2006.

CHAPTER 2

2. EXPERIMENTAL SECTION

2.1 Materials

The Collimated radiation beam of X-ray and γ-rays was used to estimate the attenuation properties of different types of composite samples which were prepared with the composition of various locally available cost effective and non-hazardous materials. In this viewpoint, raw beach sand, naturally occurring heavy minerals such as, Magnetite and Ilmenite, inland sand, dyeing sludge etc. were used as fillers to fabricate the radiation shielding blocks for testing their attenuation properties of hazardous ionizing radiations, such as, X-ray and γ-rays in the energy range of 65 keV to 1250 keV. The Madupur clay and cement were used as the binders (base matrix).

2.2 Ingredients of the Investigated Composite Materials

The preferred ingredients of those composite materials are:

(i) Beach minerals - Magnetite (M): $Fe^{2+}(Fe^{3+})_2(O^{2-})_4$
(ii) Beach minerals - Ilmenite (I): $Fe^{2+}Ti^{4+}(O^{2-})_3$
(iii) Raw beach sand (RBS)
(iv) Inland sand (Ordinary building sand) : IS
(v) Brick chip (BC)
(vi) Textile dyeing sludge (TDS)
(vii) Madhupur clay: Sticky type clay-Reddish (STC-R)
(viii) Sticky type clay-Gray (STC-G)
(ix) Portland cement
(x) Bismuth oxide (Bi_2O_3)

Among those ingredients, the proposed filler materials are M, I, RBS, TDS, OBS, BC and the matrix materialsare fine-grained STC-R (Madhupur Clay) and STC-G and cement to aggregate the composites. Bismuth oxide (Bi_2O_3) was used as an additive in the composites.

2.3 Sample Collection

2.3.1 Raw beach sand and heavy minerals (Magnetite and Ilmenite)

Raw beach sand (RBS) was collected from Kalatoli foredune area (GPS location: 21.4157 N and 91.9824 E) at the recent deposition in Cox's Bazar sea beach, Bangladesh. Heavy minerals, Magnetite and Ilmenite, were separated from recently deposited RBS in the pilot plant of Beach Sand Minerals Exploitation Centre (BSMEC) of Bangladesh Atomic Energy Commission (BAEC), Cox's Bazar. The BSMEC plant is equipped with various kinds of gravity, magnetic and electric separators. The major heavy minerals, namely Magnetite, Ilmenite are used to produce by following standard flow sheet [Figure-2.1]. Incorporating several separation procedures, below is the generalized flow chart for the collection of Magnetite and Ilmenite from raw sand.

After removing the organic and in-organic residue in the raw sand through Trammel screen, the sand slurry is passed through a Low Intensity Magnetic Separator (LIMS). LIMS is characterized by a permanent magnet with magnetic susceptibility of 15000 gauss which attracts ferromagnetic minerals, such as magnetite as a primary magnetic fraction. The primary non-magnetic fraction that contains the rest of the raw sand is transported to the gravity separator, Wilfley table for heavy mineral separation through attritioner and screw classifier for cleaning the minerals from rusting and clay attachments.

The heavily concentrated part from Wilfley table is sent to Wet High Intensity Magnetic Separator (WHIMS) as slurry. The magnetic field in WHIMS can be controlled by electricity as per the requirement to separate secondary magnetic fractions (Ilmenite and garnet concentrate). Both fractions are stored for further separation to remove water. The Ilmenite and garnet concentrate is then passed through a diesel based drum dryer to dry the minerals at 80-100^{0}C before lifting to High Tension Roll Separator (HTRS) as an electric separator to divide conductor and con-conductor fraction. Based on electric conductivity, Ilmenite is separated as a conductor fraction which needs to be purified from magnetic using a cross belt magnetic separator. Magnetite from this cross belt separator can be added to the magnetite of primary magnetic part coming out from LIMS.

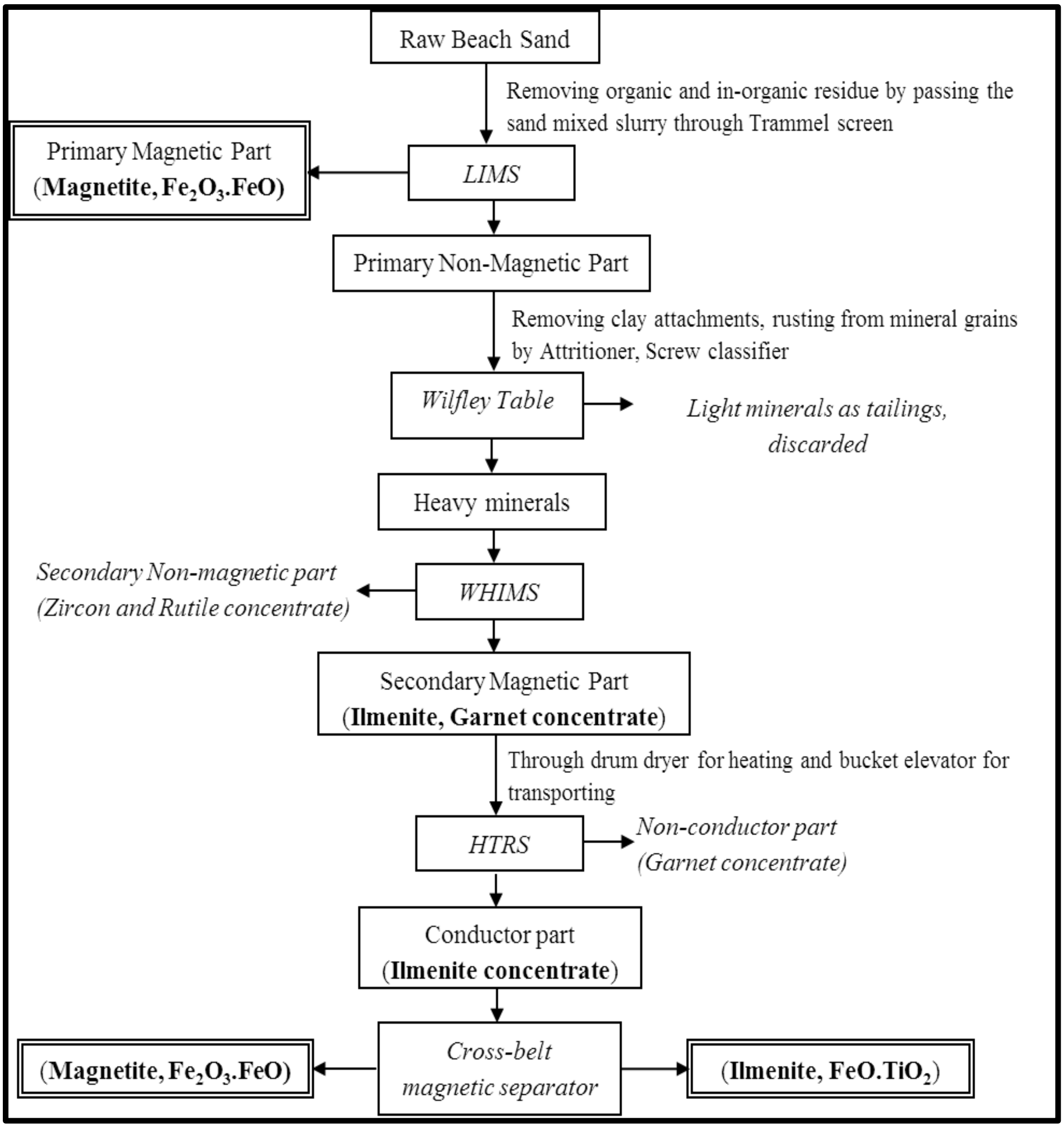

Figure-2.1: Generalized flow chart for Magnetite and Ilmenite separation from raw beach sand at pilot plant of BSMEC, Cox's Bazar

2.3.2 Madhupur clay (sticky type clay-reddish brown)

The Madupur clay sample was collected in the container from Baipayl (GPS Location: N 23.953398, E90.278878) which is located in the Madhupur Tract in Savar region, Dhaka. The colorof collected clay sample was reddish-brown.

2.3.3 Textile dyeing sludge

The textile dyeing sludge was collected from the textile industry of Dulal Brothers limited (DBL Group), Sreepur-Kashimpur Road, Shardagonj, Gazipur. Dyeing sludge was packed and stored for more than 6 months at ETP plant.

2.3.4 Portland cement

The Portland composite cement, manufactured by Holcim cement (Bangladseh) Ltd., was collected from Savar, Dhaka.The typical constituents of Portland cement clinker (plus gypsum) are shown in Table-2.

Table-2: Typical constituents of Portland cement clinker

S.N	Clinker	CCN*	Mass (%)
1.	Tricalcium silicate $(CaO)_3 \cdot SiO_2$	C3S	25-50%
2.	Dicalcium silicate $(CaO)_2 \cdot SiO_2$	C2S	20–45%
3.	Tricalcium aluminate $(CaO)_3 \cdot Al_2O_3$	C3A	5–12%
4.	Tetracalciumaluminoferrite $(CaO)_4 \cdot Al_2O_3 \cdot Fe_2O_3$	C4AF	6–12%
5.	Gypsum $CaSO_4 \cdot 2\ H_2O$	$C\overline{S}H2$	2–10%

*CCN: Clinker Chemist Number

2.3.5 Inland sandand brick chip

Inland sand and Brick chips (size: near to 1cm) were also collected from Savar, Dhaka.

2.4 Composite Sample Ingredient Preparation

Upon collection, all the samples were appropriately packed and manifested for recognition code. Then the samples were carried and stored at the sample processing laboratory of Health Physics and Radioactive Waste Management Unit (HPRWMU) in the Institute of Nuclear Science & Technology (INST), Bangladesh Atomic Energy Commission (BAEC) where the samples were processed. After slicing into small pieces, the collected samples were allowed to dry in an electric oven at 105 °C until having constant weight. The dried samples were smashed into fine grained powder with a mortar and pestle. For making a more finely grained powder and homogeneous grain size, the samples were sieved (mesh sizes were reduced to less than 100µm). Using an electrical balance the samples were weighed and the net weights of the samples were recorded. The sample-filled plastic containers were marked separately with identification number, date of preparation and net weight of the samples. The composite sample ingredient preparation steps and finely grained ingredients are presented in (Figure-2.2).

Figure-2.2: The flow diagram of composite sample ingredient (Madhupur clay) preparation steps and Finely grained ingredients ready to mold for composite block preparation

2.5 The MI, RBS, IS and RBS-DS Composite Block Fabrication

In the first-step of composite block fabrication, the mixed aggregates were placed in a concrete mixer container. The mixing ratio (by wt.) of the composite sample ingredients is given in (Table-3). Afterward, the mixed aggregates were poured into a specified dice (the molding-box) uniformly. For the convenience of experiments, the length and width of the dice were 5″ and 5″ respectively whereas the thicknesses of the composite blocks vary from 1.3″ to 4.6″ to prepare the handy specified thick samples. Manual compaction was done by metallic rod for their close-fitting, air removing and settling which resulted in the densification of the composite blocks.

Table-3: The mixing ratio (by wt.) of the composite sample ingredients

S.N.	Sample ID	Ingredient	Mixing Ratio (wt.)
1.	MI Composite	Magnetite : Ilmenite : Madhupur Clay	1 : 1 : 1
2.	RBS Composite	Raw Beach Sand : Madhupur Clay	2 : 1
3.	IS Composite	Inland Sand : Madhupur Clay	2 : 1
4.	Ordinary Concrete	Cement : Inland Sand : Brick Chip	1 : 1.5 : 3
5.	RBS-DS Composite	Raw Beach Sand : Dyeing Sludge : Clay	1 : 1 : 1

The high density of the compacted samples led to reducing the porosity. Then the dice (molding-box) was kept in a cool and dry regionat room temperature to settle-down for forty-eight hours. Then the samples were dried under the sun light for 3-4 days. Finally, the fabricated composite blocks are ready to characterize (Figure-2.3).

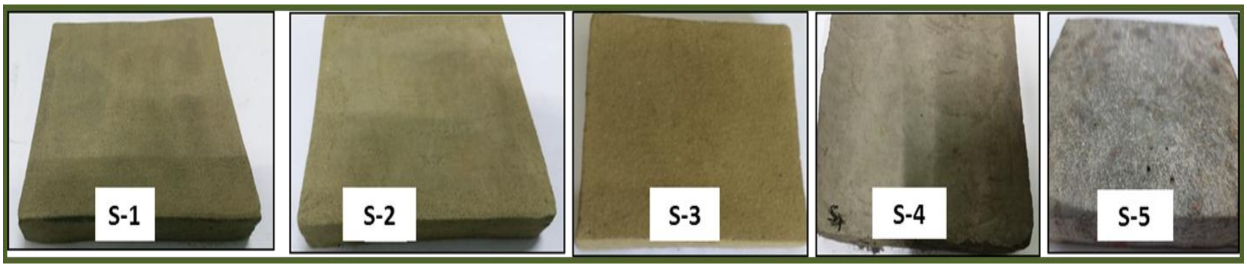

Figure-2.3: The fabricated MI (S-1), RBS (S-2), IS (S-3), RBS-DS (S-4) Composites and Ordinary Concrete (S-5)

2.6 Ordinary Concrete (OC) Preparation

Nominal mix (Cement: Sand: Aggregate) is a simple, fast way of getting the finished concrete. The mix of grade M20 (Indian standards) corresponds approximately to the mix proportion (1:1.5:3). The grade usually indicates the 28-day cube strength. The crushed stone chips in angular shape were used as coarse aggregate. Normal tap water conforming drinking quality was used for the preparation and curing of concrete specimens. The mixing ratio of cement, inland sand and stone chips were 1:1.5:3 respectively.The physical densities of the corresponding samples (composite blocks) were determined by the conventional (gravimetric) method.

2.7 Experimental Details of Radiation Attenuation Analysis

The mono-energetic collimated radiation beams of X-ray and gamma-ray sources were applied to estimate the shielding potential of different types of composite-samples such as MI-composite, RBS composite, IS-composite, RBS-DS Composite, ordinary concrete. The fabricated composite and concrete blocks were used to examine the radiation attenuation capacity for both relatively low and high energy ionizing radiation.

The samples were exposed by radiation photons emitted from relatively low energy X-ray (65-164 keV), moderate energy ^{137}Cs (661.6 keV) and relatively high energy ^{60}Co (1,173.2 keV & 1,332.5 keV; average energy of 1250 keV) at the Secondary Standard Dosimetry Laboratory (SSDL) of Bangladesh Atomic Energy Commission, Savar, Dhaka. The linear and mass attenuation measurements of the prepared samples were performed using broad beam X-ray and gamma-ray transmission geometry [1-3]. The experimental set-up of the transmission geometry used in the current study is shown in Figure-2.4 & Figure-2.5.

Figure-2.4: Experimental set-up and Control Panel of X-ray attenuation analysis

The source was enclosed in a lead container with one face hole of 5.5 mm, located behind the source collimator. The source to surface distance (SSD) of experiment was kept in 100 cm. In the present experiments, detector was located relatively at distant point (i.e., 100 cm) from the sample in order to ensure the measurement of the attenuated secondary beam that escaped after the interaction with the sample.

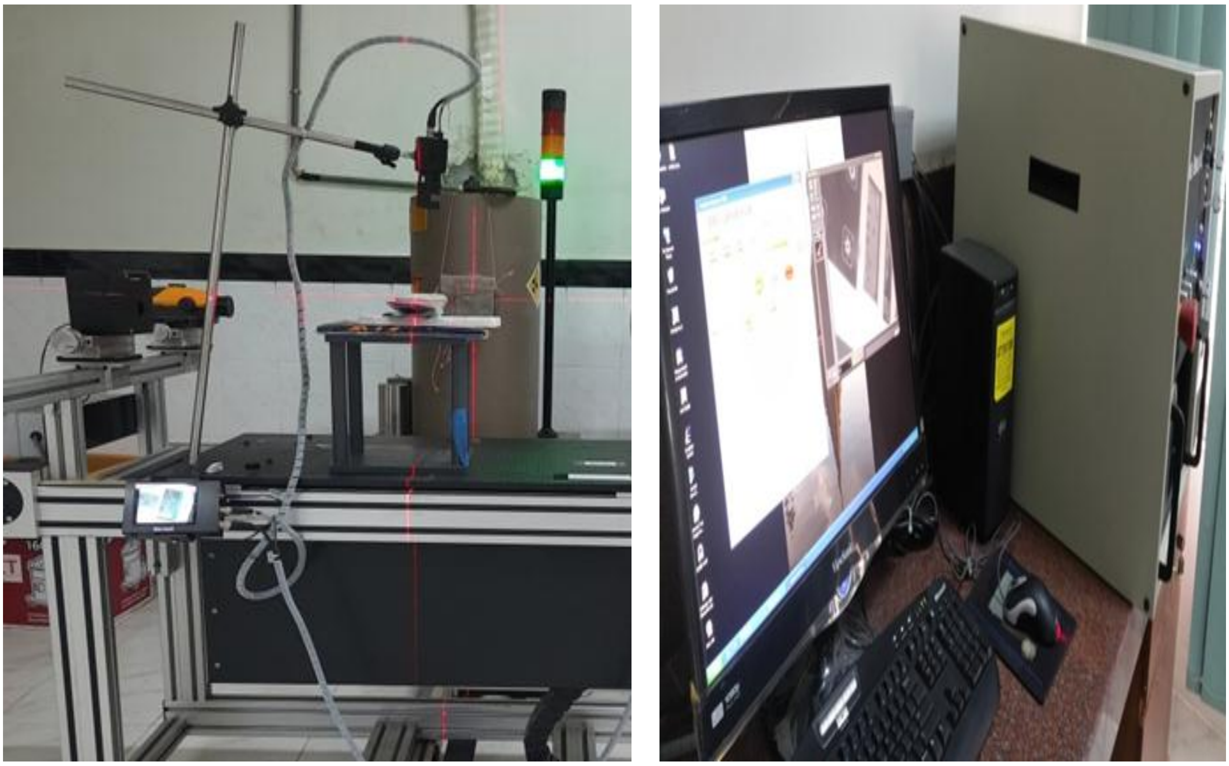

Figure-2.5: Experimental set-up and Control Panel of γ-ray attenuation analysis

A Geiger-Müller (GM) radiation determining detector was employed to investigate the radiation attenuation efficacy of the prepared sample materials [4]. The incident and transmitted radiation (X-ray and gamma-ray) intensities were measured by using a GM radiation measuring detector (CANBERRA - RADIAGEM 2000) (Figure-2.6). A series of X-ray beam qualities were selected to match the beam qualities offered by International Bureau of Weight and Measures and based on ISO narrow spectrum series. The beam current was maintained at 5 mA. The constant potential X-ray systems type Model X80-225 X-ray Beam Irradiator with a 225 kV tube was used to generate ISO narrow spectrum series X-ray reference radiation for this study.

The incident radiation beam (for X-ray and gamma-ray) data was noted without employing any sample on the collimator line. Then, the transmitted radiation beam (for X-ray and gamma-ray) data was noted for all the fabricated composite samples. The variety in radiation attenuation performance of the composite block was justified as per the variance in material compositions and thicknesses of respective sample.The obtained results were further analyzed mathematically to determine the shielding performance parameters to evaluate the shielding efficacy of the studied samples.

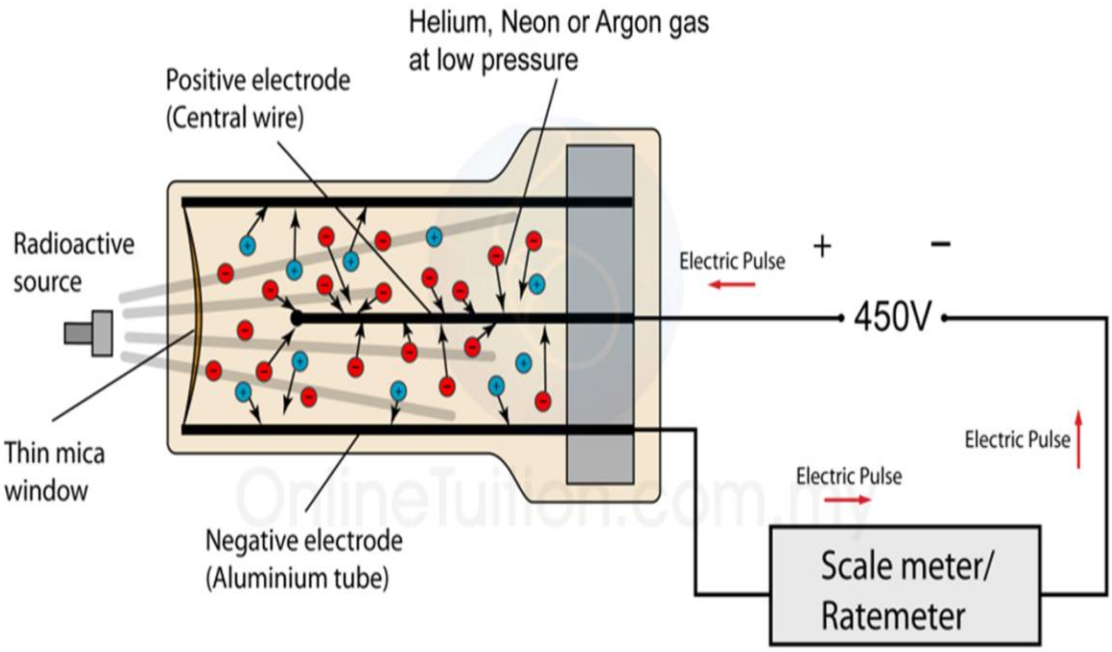

Figure-2.6: The Geiger–Muller (GM) counter for radiation detection

The entire experimental apparatus was also placed at a proper distance from the walls of the room so as to avoid the influence of scattered photons from the wall.

2.8 Experiment of Neutron Activation Analysis (NAA)

To determine elemental concentrations of the samples, TRIGA MARK-II Research Reactor (3MW Thermal Power, 7.1×10^{13} Thermal Neutron Flux at Dry Central thimble, 0.025 eV Thermal Neutron Energy) was used for the Neutron Activation Analysis (NAA).

2.8.1 NAA sample preparation

Almost, fifty (50) mg of each dried powder sample was weighed in polyethylene-bag and heat sealed (double pack). Aimed at relative standardization approach, one standard reference material NIST-1633b (coal-fly-ash) was used in this investigation. The standard was prepared the same manner as the prospective samples. Samples and standard were taken in a glass-vial for irradiation at nuclear reactor [5].

2.8.2 Neutron irradiation scheme

At the 3MW TRIGA Mark–II Nuclear Research Reactor of Bangladesh Atomic Energy Commission (BAEC), Savar, two irradiation patterns were performed using pneumatic transfer (rabbit) system:

(a) The short-irradiation patternwas doneindependently for each sample with the thermal-neutron flux 5.28×10^{12} $n \cdot cm^{-2} \cdot s^{-1}$ (for 60 seconds at 250 kW)

(b) The long-irradiation pattern was doneconcurrentlyfor all samplesas well as standards with the thermal-neutron flux 2.11×10^{13} $n \cdot cm^{-2} \cdot s^{-1}$ (for 14 minutes at 1 MW).

To estimate the neutron flux gradient within the sample-stack, three IRMM-530RA Al - 0.1% Au (0.1 mm foil) monitor foils were also irradiated at nuclear reactor by employing them at the bottom, middle and top of the sample-stack for the long-irradiation pattern. The Cross sectional view of the reactor neutrons for NAA Experiment is shown in Figure-2.7.

2.8.3 The γ-ray counting

After irradiation at nuclear reactor, the γ-ray counting was completed with a high-purity germanium (HPGe) detector [1.8keV resolution at 1332.5keV of ^{60}Co,25 % efficiency relative to a NaI(Tl) detector; CANBERRA] coupled with a digital gamma-spectrometer (ORTEC, DSPEC Jr™). At short-irradiationpattern, first-counting was taken for 300 seconds after a decay time of about 300 seconds and second-counting for 600 seconds after a decay time of 2–3 hours.

At long-irradiated samples, first counting was taken for 40 minutes after a decay time of 2 days, second counting was taken for 2 hours after a decay time of 7–10 days and third counting was taken for 8–12 hours after a decay time of 14–21 days.

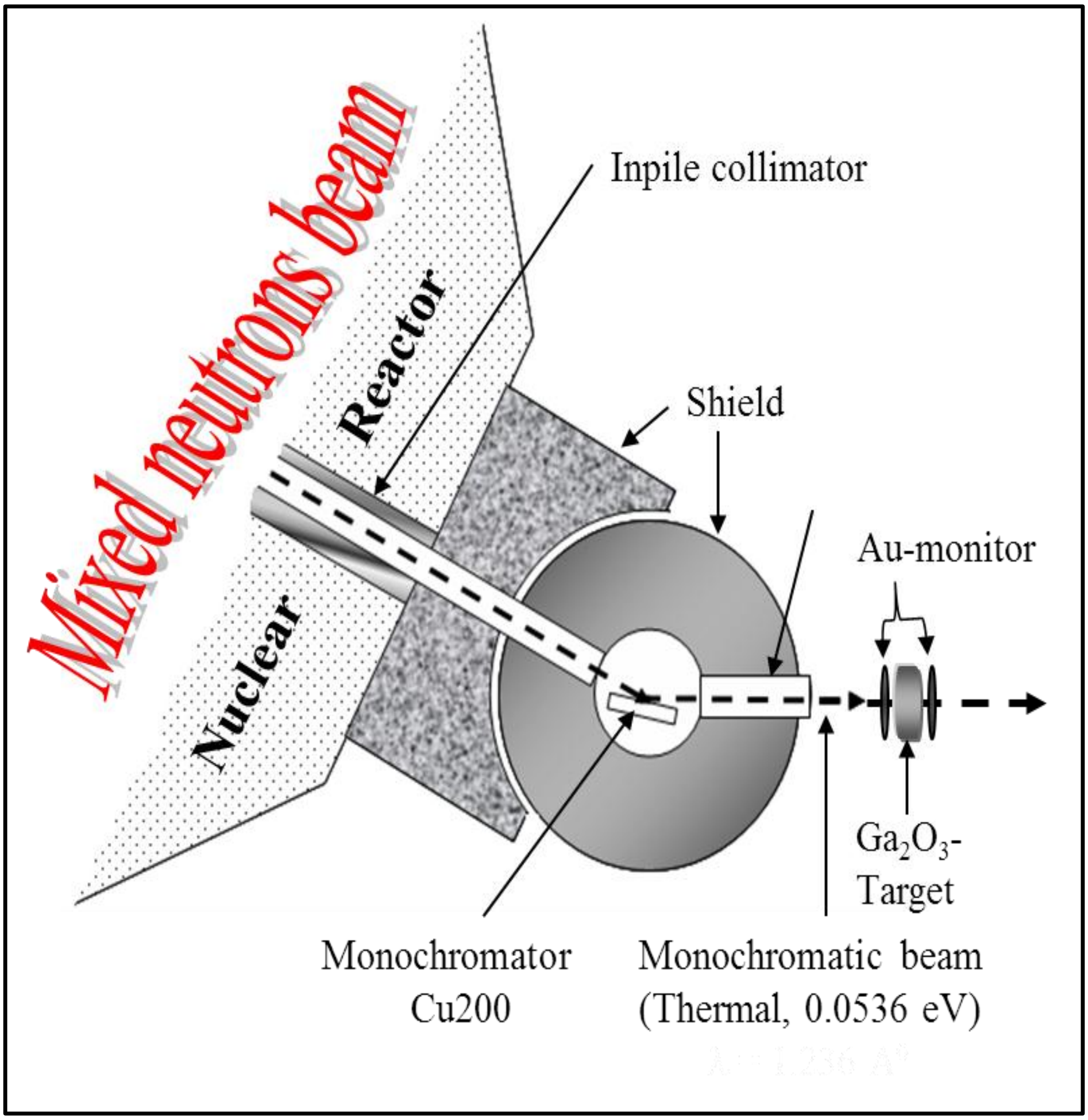

Figure-2.7: Cross sectional view of the reactor neutron beam for NAA Experiment

Radionuclides having short half-life and long half-life were detected from the short and long irradiation pattern respectively by comparative-method. The HPGe detector (CANBERRA) with digital γ-spectrometry arrangement was shown in the Figure-2.8.

Figure-2.8: Canberra HPGe detector with digital γ-spectrometry system

2.9 Experiment of Neutron Radiography

Neutron radiography (NR) technique has been used for the morphological investigation of composite block which exhibits a neutron image of the internal details of an object by the selective absorption of a neutron beam. The NR provides a very efficient tool for investigations in the field of non-destructive testing. The basic principle of NR is analogouswith the radiography of X-ray. A neutron beam hits on a sample and after passing through the sample the neutron leave their image on a photographic-film. The NR follows the basic principles of radiography whereby a beam of radiation is modified by an object in its path and the emergent beam is recorded on a detector.

Thus, the NR involves three principal components:

1. A suitable neutron beam
2. An object of radiographic interest
3. A device to record the transmitted radiation

The Thermal Neutron Radiography Facility (TNRF) has been fixed in the tangential beam port of the 3MW TRIGA MARK-II research reactor at the Center for Research Reactor (CRR), Atomic Energy Research Establishment, Savar, Dhaka. The Schematic View of TNR Set-up at TRIGA Mark-II Research Reactor is shown in figure-2.9.

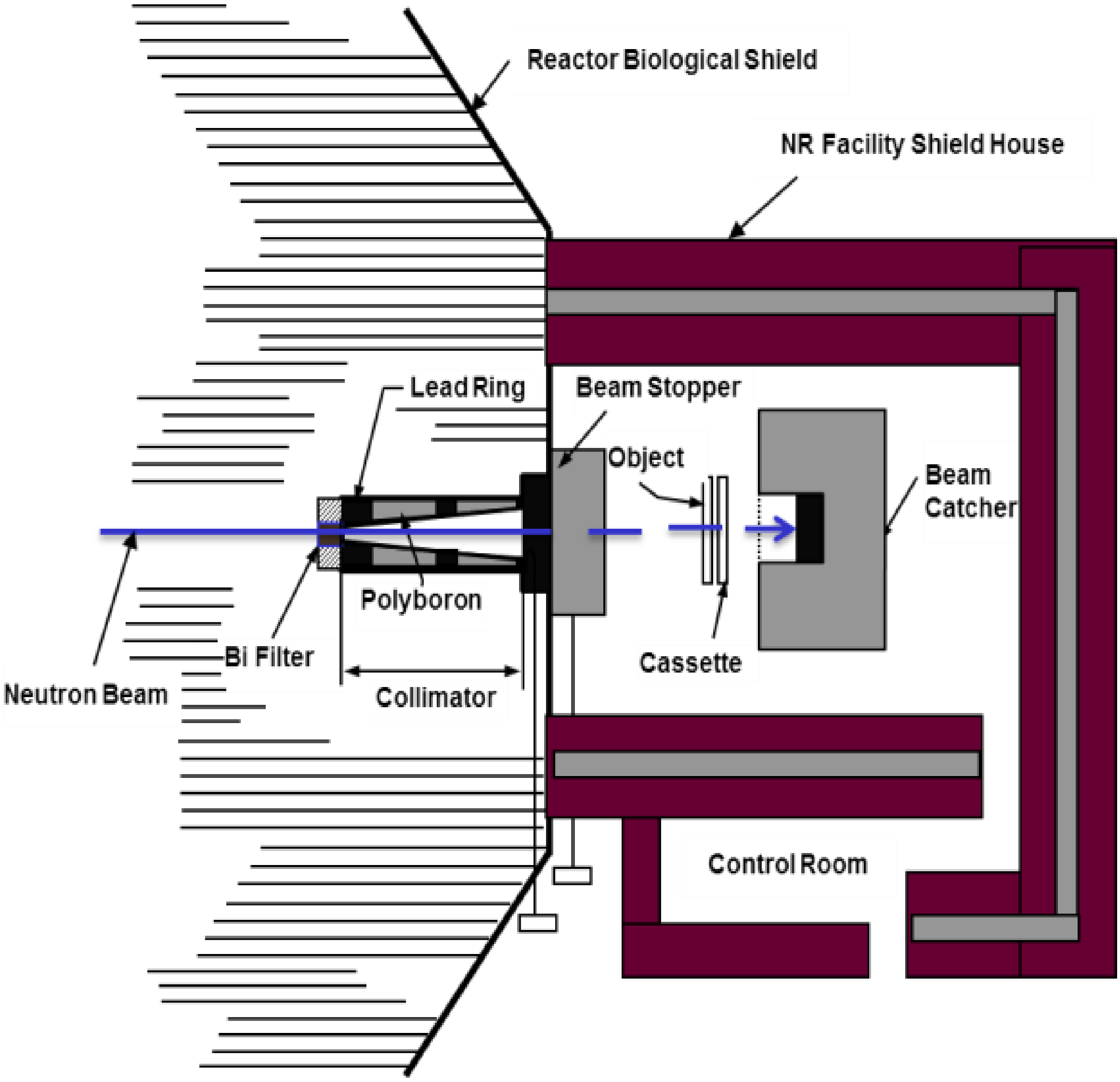

Figure-2.9: Schematic View of TNR Set-up

The tangential beam port has been used for the neutron radiography work because of its less amount of gamma ray emission compared to other beam ports and also because of its sufficient thermal neutron flux. The TNRF consists of Bi-filter, cylindrical divergent collimator, a beam stopper, a sample and camera holder table, a beam catcher and a biological shielding house. The Tangential beam port of TNRF at TRIGA Mark-II Research Reactor is shown in figure-2.10.

2.9.1 Image recording

The photographic films were applied for image recording of the materials in neutron radiography technique. Hence, no special films are available for neutron radiography and the standard X-ray films are normally used for this experiment.

Figure-2.10: The Tangential beam port of TNRF at TRIGA Mark-II Research Reactor

2.9.2 Neutron imaging by converter materials

As neutron is a chargeless particle, the photographic films are insensitive to them. Therefore, producing a neutron image, it is necessary to use a foil/screen which converts the transmitted neutron into another type of detectable radiation like, alpha, beta, gamma radiation or light and it is the secondary radiation which is detected by a photographic film or other detector. Hence, the metal foils of gadolinium (Gd) were used as a converter material in this experiment. In direct method the photographic film is placed in contact with the metallic gadolinium converter inside the neutron radiography cassette and the cassette is placed directly in the neutron beam. The radiation emitted from the foil then produces an image on the film [6-9].

2.10 Characterization of Mechanical Properties

The mechanical properties (such as tensile strength, bending strength) of the materials were measured by Universal Testing Machine at Nuclear and Radiation Chemistry

Division (NRCD), BAEC, Savar, Dhaka which was shown in figure-2.11. The moisture absorption will be detected by weighing method and the crack/hole of the materials will be detected by neutron radiography method.

Figure-2.11: Universal Tensile Strength measuring machine

2.11 Theoretical Factors and Parameters

2.11.1 The radiation-matter interaction (RMI) for the X-ray and γ-ray

The X-ray and γ-ray photons interact with the matter (electrons, nucleons, electric field surrounding nuclei/electrons etc.) via a series of mechanisms, which can be categorized according to the type of object-materials and the result of the interaction on the photon (absorption/scattering) [10,11]. At the energies beyond the UV range, the leading RMI-processes are photoelectric effect/absorption, Compton scattering (incoherent scattering), and pair production.Figure-2.12 shows a graphical demonstration on these processes for X-ray and γ-ray photon.

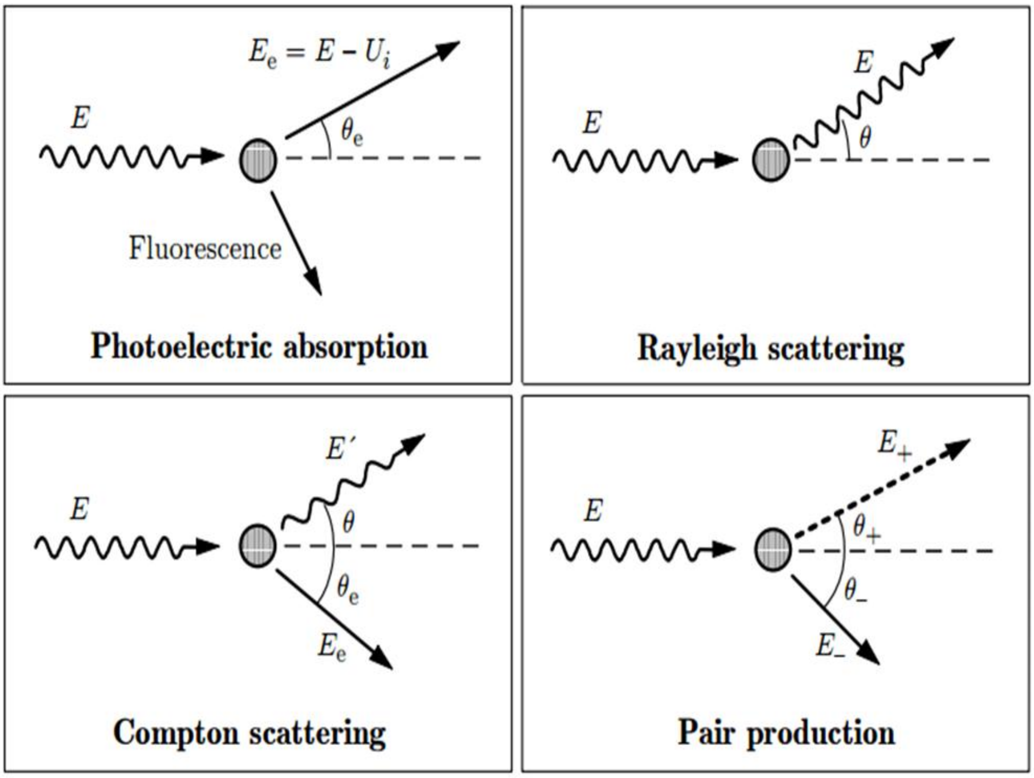

Figure-2.12: Various effects due to the "Radiation Matter Interaction".
https://www.oecd-nea.org/upload/docs/application/pdf/2020-01/nsc-doc2015-3.pdf

2.11.2 The photoelectric absorption RMI

In a photoelectric absorption interaction, the incident-photon vanishes and its energy is shifted to the target atom (or cluster of atoms) [10,11]. The threshold energy for this route to occur depends upon the binding energy of the electron in a specific shell. The Cross-section for photoelectric effect/absorption strongly depends on atomic number of an element. The intensity "I" of a monochromatic beam of photons with energy "E" thus losses exponentially as a function of the penetration depth "x" in a material,

$$I\,(x) = I_0 e^{-\mu x} \qquad (1)$$

where, the attenuation coefficient "μ" is proportional to the atomic density "N" of the medium and the photoabsorption cross section "σ_γ",

$$\mu (E) = N\sigma_\gamma (E) \quad (2)$$

2.11.3 The compton scattering RMI

The compton scattering RMI is the route of inelastic/incoherent scattering of gamma-ray photon while interacting with an electron. This scattering refers to the collision of a photon with a weakly bound electron, whereby the photon transfers part of its energy to the electron and is deflected with respect to its original direction of propagation [10,11]. The cross-section for Compton scattering route is minimum dependent on atomic number and slowly decreases with the increase in the energy of the radiation. Hence, this process is dominant at intermediate photon energy for all elements. The photon energy (E) is large compared to the electron's binding energy. Due to conservation of energy and momentum, the photon energy (E′) after the collision and the scattering angle (θ) of the photon are then related by

$$E' = mc^2 / \{1 - \cos\theta + (1/u)\} \quad (3)$$

Where, $u = E/mc^2$ is the photon energy (before the collision) in units of the electron rest energy. The kinetic energy ($T = E - E'$) imparted to the electron is biggest for a head-on collision ($\theta = \pi$).

2.11.4 The pair production RMI

The pair production RMI is the transformation of a photon into an electron-positron pair. For photon energies exceeding $2mc^2$ (1.022 MeV), an interaction mechanism becomes possible where the inward photon disappears and an electron-positron pair, with a total energy equal to the photon energy (E), is generated. To conserve momentum, this can only occur in the presence of a third body, usually a nucleus. Any excess energy carried by the photon goes into the kinetic energy shared by the pair. Hence, it is a dominant process for heavy elements at higher photon energies [10,11]. At high photon energies, the electron-positron pair is producedfavorably in the forward direction. The absorption coefficient due to pair production can be estimated by the equation of

$$\mu = N\sigma^{\text{(pair production)}}. \quad (4)$$

This process is the best example for transformation of energy into mass. The cross-section for pair production in the electric field of a nucleus varies directly with atomic number.

2.11.5 The LAC parameter

The linear attenuation coefficients are one of the important parameters explaining the interaction of matter and radiation. The intensity of the radiation-beam would be attenuated according to the Beer-Lambert's principle when γ-ray beam crosses an absorber. The linear attenuation coefficient μ_L (cm^{-1}) can be derived from the Lambert-Beer law [12-15]. In current study, the attenuation of the transmitted photon intensity (γ-ray and X-ray) through the absorbing constituents is described by this rule as (Eq.-5):

- **Linear Attenuation Coefficient (LAC),** $\mu_L = \frac{1}{x} \ln (I_O/I)$ (5)

Where I_o and I_t are the incident and transmitted radiation beam intensities, μ_L (cm^{-1}) is the linear attenuation coefficient and x is the thickness of the material (cm).

2.11.6 The MAC parameter

The measured linear attenuation coefficient is used to determine the mass attenuation coefficients μ_m (cm^2/g) by applying the bulk densities of the respective samples as follows (Eq.-6):

- **Mass Attenuation Co-efficient (MAC),** $\mu_m = \frac{\mu}{\rho} = \frac{1}{\rho x} \ln (I_O/I)$ (6)

The linear attenuation coefficient reveals the absorption of photons from a mono-energetic radiation beam by interaction with the materials [12-15]. The greater density of the composites can cause more interaction of the X-ray and gamma ray photons. Thickness and Photon Energy are the main parameters that affect the linear attenuation coefficient (LAC). Thickness, photon energy and density are the main parameters that affect the MAC. The linear attenuation coefficient is strongly energy dependent. In general, lower energetic gamma photons have a higher interaction probability, and hence cause relatively high attenuation. The photon beam transmission was considered in the relatively low to high energy range of 65 – 1250 keV to verify the shielding applicability of the studied samples.

2.11.7 The half value layer (HVL) parameter

The thickness of any given material where 50% of the incident energy has been attenuated is known as the half-value layer (Figure-2.13). The HVL is expressed in units of distance (mm or cm). Like the attenuation coefficient, it is photon energy dependent. Increasing the penetrating energy of a stream of photons will result in an increase in a material's HVL. The HVL is inversely proportional to the attenuation coefficient [12-15]. The HVL is often used in radiography simply because it is easier to remember values and perform simple calculations. In a shielding calculation, such as illustrated to the right, it can be seen that if the thickness of one HVL is known, it is possible to quickly determine how much material is needed to reduce the intensity to less than 1%.The half value layers (HVL) of the studied composite materials were determined based on the investigationalclarifications. The half value layer (HVL) is expressed as (Eq.-7):

❑ **Half Value Layer (HVL),** $$\mathrm{HVL} = \ln 2/\mu_L \qquad (7)$$

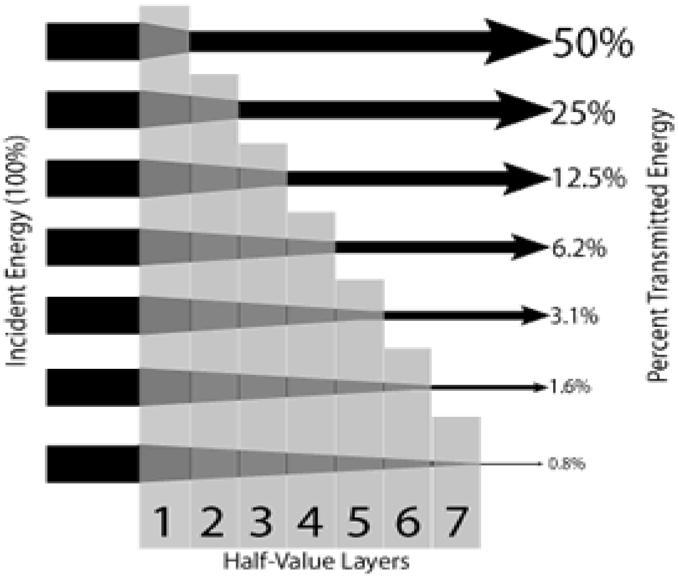

Figure-2.13: Graphical exhibition of HVL.

References:

[1] H. A. Jahagirdar, B. Hanumaiah and B. R. Thontadarya, "Determination of narrow beam attenuation coefficients from broad beam geometrical configuration for 320KeV photons", *Int., Appli. Radiat. Isot,* Vol.43, pp.1511, 1992

[2] International Atomic Energy Agency (IAEA), "Applying radiation safety standards in diagnostic radiology and interventional procedures using X rays", IAEA Safety Reports, Series No. 39, October 2006.

[3] K. D. Steidley, "Structural Shielding Design and Evaluation for Medical Use of X-Rays and Gamma Rays of Energies Up to 10 MeV", J. Nucl. Med. Technol., NCRP Report No. 49, 5(2):107, 1977;

[4] D. D. Bradley, C.S. Chong, A. Shukri, A.A. Tajuddin A. M. and Ghose, "A new method for the direct measurement of the energy absorption coefficient of gamma rays", *Nucl. Instrum.Meth.Phys. Res.*, A. 280 - 392, 1989

[5] Rahat Khan*, Md. Shohel Parvez, Umma Tamim, Sopan Das, Mohammad Amirul Islam, Kamrun Naher, Md. Harunor Rashid Khan, Farzana Nahid and Syed Mohammod Hossain, "Assessment of rare earth elements, Th and U profile of a site for a potential coal based power plant by instrumental neutron activation analysis", *Radiochim. Acta, DE GRUYTER*, pp. 1-10, 2018; aop, https://doi.org/10.1515/ract-2017-2867

[6] Sujatha Pai, Indra J. Das, James F. Dempsey, Kwok L. Lam, Thomas J. LoSasso, Arthur J. Olch, Jatinder R. Palta, Lawrence E. Reinstein, Dan Ritta, Ellen E. Wilcox, "TG-69: Radiographic film for megavoltage beam dosimetry", *Am. Assoc. Phys. Med, Medical Physics*, Vol. 34, No. 6, pp. 2228-2256, June 2007

[7] B. G. Akdeniz, G. Lomcali, "Densitometric evaluation of four radiographic processing solutions", *Dentomaxillofac. Radiol.,* 27:102-6, 1998.

[8] S Eikenberg, R. Vandre, "Comparison of digital dental X-ray systems with self-developing film and manual processing for endodontic file length determination", *J Endod,* Vol. 26:65-7, 2000

[9] E. L. Kitts, “The AAPM/RSNA physics tutorial for residents: physics and chemistry of film and processing”, *Radiographics*, Vol.16:1467, 1996.

[10] Christian W. Fabjan, Herwig Schopper, Detectors for Particles and Radiation, “Particle Physics Reference Library, Springer”, Vol. 2, pp. 6-12, 2020 (ISBN 978-3-030-35317-9, https://doi.org/10.1007/978-3-030-35318-6)

[11] F. Salvat, “PENELOPE-2014: A Code System for Monte Carlo Simulation of Electron and Photon”, Transport Book, NEA Data Bank, OECD, Nuclear Energy Agency, Barcelona, Spain, Vol. 3, PP. 49-75, 2015.

[12] P. Jacob, R. Meckbach, “Shielding factors and external dose evaluation”, *Radiat. Prot. Dosim.*, Vol.21 (1/3), pp.79–85, 1987

[13] I. I. Bashter, “Calculation of Radiation attenuation coefficients for shielding concretes”, *Ann. Nucl. Energy*, Vol. 24 (17), pp. 1389-1401, 1997

[14] Ripan Biswas, Hossain Sahadath, Abdus Sattar Mollah, Md. Fazlul Huq,”Calculation of gamma-ray attenuation parameters for locally developed shielding material: Polyboron”, *Journal of Radiation Research and Applied Sciences, ElSEVIER,* Vol. 9, pp. 26-34, 2016

[15] J. H. Hubbel, “Photon mass attenuation and energy absorption coefficients from 1 keV to 20 keV”, *Appli. Radiat.Isot*., 33, 1269, 1982

CHAPTER 3

3. RESULTS AND DISCUSSION

3.1: Preparation of radiation shielding materials

The current study emphasizes the preparation of the various locally available, cost effective and non-hazardous composites for the X-ray and γ-rayattenuation. The attenuation behavior depends on the density and chemical composition of the material and photon energy of the ionizing radiation. On this basis, an attempt was taken to design and fabricate a high density material having heavy elemental composition and characterize their attenuation properties at the energy range of 65 keV to 1250 keV for X-ray and γ-ray. In this perspective, raw beach sand (having heavy elemental composition), naturally occurring heavy minerals such as, Magnetite and Ilmenite were selected as the targeted filler to fabricate the radiation shielding blocks for testing their attenuation properties. Moreover, inland sand and textile dyeing sludge (TDS) were also evaluated as base matrix. The bismuth oxide (Bi_2O_3), a high density ingredient, was incorporated as an additive to mark a comparison. The TDS has an impact of environmental burden. The effluents discharged from textile factories are a mixture of dyes, metals and other pollutants [1]. The colorants can be divided into natural and synthetic dyes. Synthetic dyes are produced easily, in different colors, and characterized by their fastness, which makes them more widely used than natural dyes. The Madupur clay and cement were used as the binder (base matrix).Madhupur Clay is highly weathered and deeply oxidized reddish brown deposit exposed in the Madhupur, Barind and Lalmai Hill areas which are being aged of about 0.97 to 0.90 million years. The Madhupur and the Barind Tracts represent a tectonically uplifted surface of the red bed islands in the Bengal Basin. The high land of the Madhupur Tract in the Dhaka city and Savar area represents the Madhupur Clay Formation, the oldest exposed rock of the area [2, 3]. The Portland cement is the basic ingredient of concrete which consists of a mixture of oxides of calcium, silicon and aluminum. Portland cement and similar materials are made by heating limestone (a source of calcium) with clay and then grinding this product (called clinker) with a source of sulfate (most common gypsum) [4]. Finally, the attenuation capacities in terms of LAC, MAC and HVL of all types of fabricated composites were assessed with ordinary concrete. The biological hazard assessments were also evaluated as EDR factors.

The key elemental composition of the prospective materials was performed by neutron activation analysis (NAA) to identify the heavy elements and their impacts on radiation–matter interactions (RMI). The current morphological study by Neutron Imaging has shown the entire internal structure and arrangement of several centimeters, because of neutron penetration efficacy.

3.2 The LAC Values Analysis

The comparative assessments of radiation attenuation capability in terms of liner attenuation coefficient (LAC) are exhibited between the fabricated composite material and the conventional radiation-shielding material (ordinary concrete) for X-ray and γ-ray photons of ^{137}Cs and ^{60}Co.

3.2.1 The X-ray LAC

The experimental LAC of the MI, RBS, IS, Ordinary Concrete and DS Composite samples through the energy range 65 keV to 164 keV of X-rays are exhibited in Figure-3.1. Amongst the composite samples, the MI composite shows the highest LAC values. The LAC of M-I composite material decreases from 1.6644±0.007 cm^{-1} to 0.4467±0.004 cm^{-1} for 65 keV to 164 keV X-rays respectively. The LAC of RBS composite drops from 1.4026±0.005 cm^{-1} to 0.4050±0.002 cm^{-1} for 65 keV to 164 keV, respectively. For 65 keV to 164 keV X-ray, the IS composite and DS composite, these two types of composites, showed the lowest attenuation capacity, the LAC falls from 0.5151±0.002 cm^{-1} to 0.2535± 0.003 cm^{-1} and 0.5134±0.004 cm^{-1} to 0.2443±0.005 cm^{-1}, respectively. The LAC values of the investigated composite materials were compared with the conventional shielding material, ordinary concrete. The ordinary concrete exhibits the moderate LAC values of 0.7189±0.003 cm^{-1} to 0.3360±0.002 cm^{-1} for 65 keV to 164 keV X-rays respectively.

At the Low mono-energetic Photon Region, the LAC values drop exponentially, while, they decrease gradually in the high photon energy region. The MI & RBS composites exhibit excellent radiation attenuation behavior among the studied composites at the low photon energy level of X-ray. The IS & DS composites show an inferior attenuation property than that of ordinary concrete.

3.2.2 The γ-ray LAC

The Liner attenuation coefficients (LAC) of the MI, RBS, IS, Ordinary Concrete and DS Composite samples through the energy range 661.6 keV to 1250 keV of γ-rays are exhibited in Figure-3.1. Amongst the composite samples, the MI composite shows the highest LAC values. The LAC of M-I composite material decreases from 0.227 cm^{-1} to 0.1460 cm^{-1} for 661.6 keV to 1250 keV γ-rays respectively.

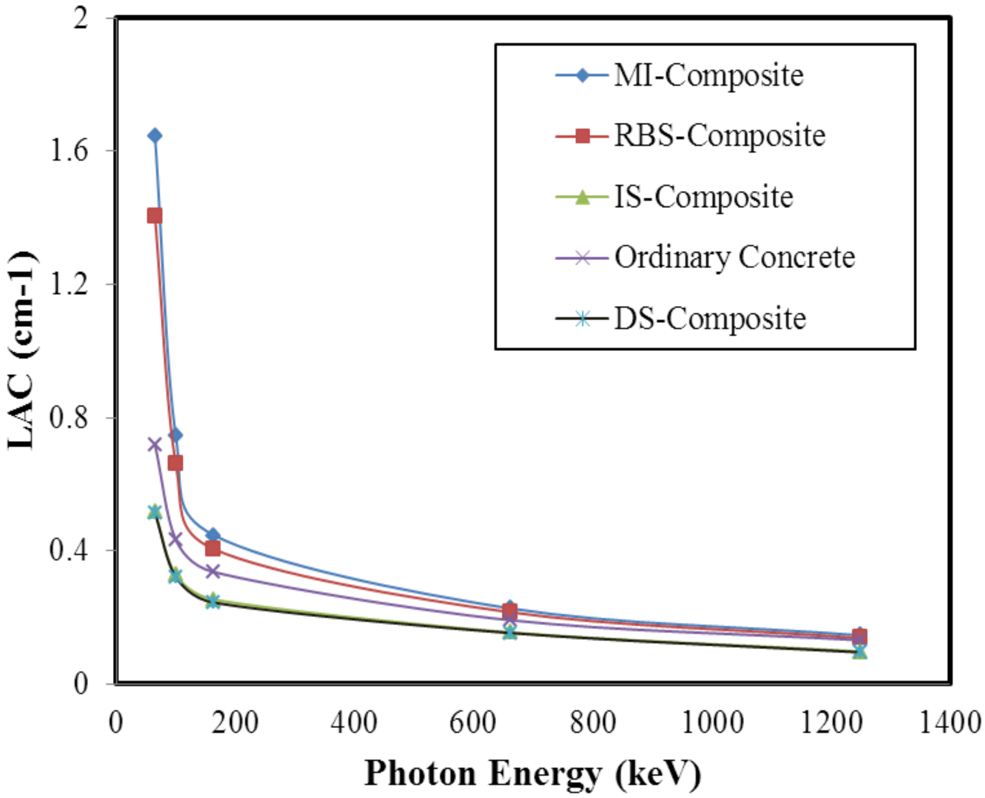

Figure-3.1: Photon Energy (keV) Vs. LAC (cm^{-1})

The LAC of RBS composite drops from 0.2156 ±0.004 cm^{-1} to 0.1378±0.002 cm^{-1} for 661.6 keV to 1250 keV, respectively. For 661.6 keV to 1250 keV γ-rays, the IS composite and DS composite, these two types of composites, showed the lowest attenuation capacity, the LAC falls from 0.1551±0.004 cm^{-1} to 0.0975± 0.003 cm^{-1} and 0.1534± 0.002 cm^{-1} to 0.0950± 0.003 cm^{-1}, respectively. The ordinary concrete exhibits the moderate LAC values (0.7189±0.003 cm^{-1} to 0.3360±0.002 cm^{-1}) for 661.6 keV to 1250 keV of γ-rays, respectively. Due to the brittleness and poor attenuation behavior, further investigations were not being done for DS composite.

3.3 Comparison in Density of the Composite Materials

The density of the fabricated composite samples was measured earlier to the succeeding experimental assessment. The measured density data is exhibitedin Table-4, which shows the density disparity among the prepared composite blocks. The maximum density of 2.77 (g/cm^3) was reached in the case of MI-composite block. Whereas, the density value (2.636 g/cm^3) of RBS composite block was slightly lower than that of MI composite. With respect to the density value (2.376 g/cm^3) of ordinary concrete, IS composite block has the lowest density value of 1.985 g/cm^3. Hence, this experimental observation clearly shows that the investigated samples of the beach mineral (MI) and RBS composites have relatively higher density in contrast with the ordinary concrete.

3.4 The MAC Values Analysis

The comparative assessments of radiation attenuation capability in terms of liner attenuation coefficient (LAC) are exhibited between the fabricated composite material and the conventional shielding material (ordinary concrete) for X-ray and γ-ray photons of ^{137}Cs and ^{60}Co. After measuring the densities of the above-mentioned composite blocks, the mass attenuation coefficient (MAC) was determined, and presented in (Figure-3.2) for the ionizing radiation of X-ray and γ-ray.

3.4.1 The X-ray MAC

The MI composite shows the highest MAC values. The MAC of M-I composite material decreases 0.592516649 $cm^2g^{-1}$to 0.160972349 $cm^2g^{-1}$for 65 keV to 164 keV X-rays respectively (Table-4). The MAC of RBS composite drops 0.532084643 cm^2g^{-1} to 0.153650706 cm^2g^{-1} for 65 keV to 164 keV, respectively. For 65 keV to 164 keV X-ray, the IS composite showed the lowest attenuation capacity, the MAC falls from 0.259409665 cm^2g^{-1} to 0.133448863 cm^2g^{-1} respectively. The MAC values of the investigated composite materials were compared with the conventional shielding material, ordinary concrete. The ordinary concrete exhibits the moderate MAC values of 0.302481145 cm^2g^{-1} to 0.141377884 cm^2g^{-1} for 65 keV to 164 keV X-rays respectively.

3.4.2 The γ-ray MAC

The MAC of M-I composite material decreases from 0.081802756 cm^2g^{-1} to 0.05260628 cm^2g^{-1} for 661.6 keV to 1250 keV γ-rays respectively (Table-4).

Table-4: The MAC Values (at various photon energies of X-ray and γ-ray) and densities of the fabricated composites.

Energy (keV)	MAC (cm^2g^{-1})			
	MI-Composite (Density: 2.77 g/cm^3)	**RBS-Composite** (Density: 2.64 g/cm^3)	**IS-Composite** (Density: 1.98 g/cm^3)	**Ordinary Concrete** (Density: 2.38 g/cm^3)
65	0.592516649	0.532084643	0.259409665	0.302481145
100	0.26805864	0.250606741	0.164746273	0.182110045
164	0.160972349	0.153650706	0.133448863	0.141377884
661.6	0.081802756	0.081805152	0.071391759	0.080689647
1250	0.05260628	0.05227227	0.042086455	0.051301218

The MAC of RBS composite drops 0.081805152cm^2g^{-1} to 0.05227227 cm^2g^{-1} for 661.6 keV to 1250 keV, respectively. For 661.6 keV to 1250 keV γ-rays, the IS composite showed the lowest attenuation capacity, the MAC falls down from 0.071391759cm^2g^{-1} to 0.042086455 cm^2g^{-1} respectively. The ordinary concrete exhibits the moderate MAC values (0.080689647 cm^2g^{-1} to 0.051301218 cm^2g^{-1}) for 661.6 keV to 1250 keV of γ-rays, respectively.

3.5 Evaluation of the LAC, MAC

The present study illustrates that the shielding effectiveness of any shielding material depends on photon energy, density and the types of chemical composition of the elements that it contains. In general, the linear and mass attenuation coefficient is sturdily energy dependent. The lower-energetic photons have agreater interaction possibility; and hence cause relatively high attenuation. The results have shown an inverse relationship between the LAC, MAC values and photon energy. The figure-3.1 exhibits that the LAC of the samples decreases as the photon energy escalations. The MAC of the investigated composites follows the LAC patterns (Figure-3.2).

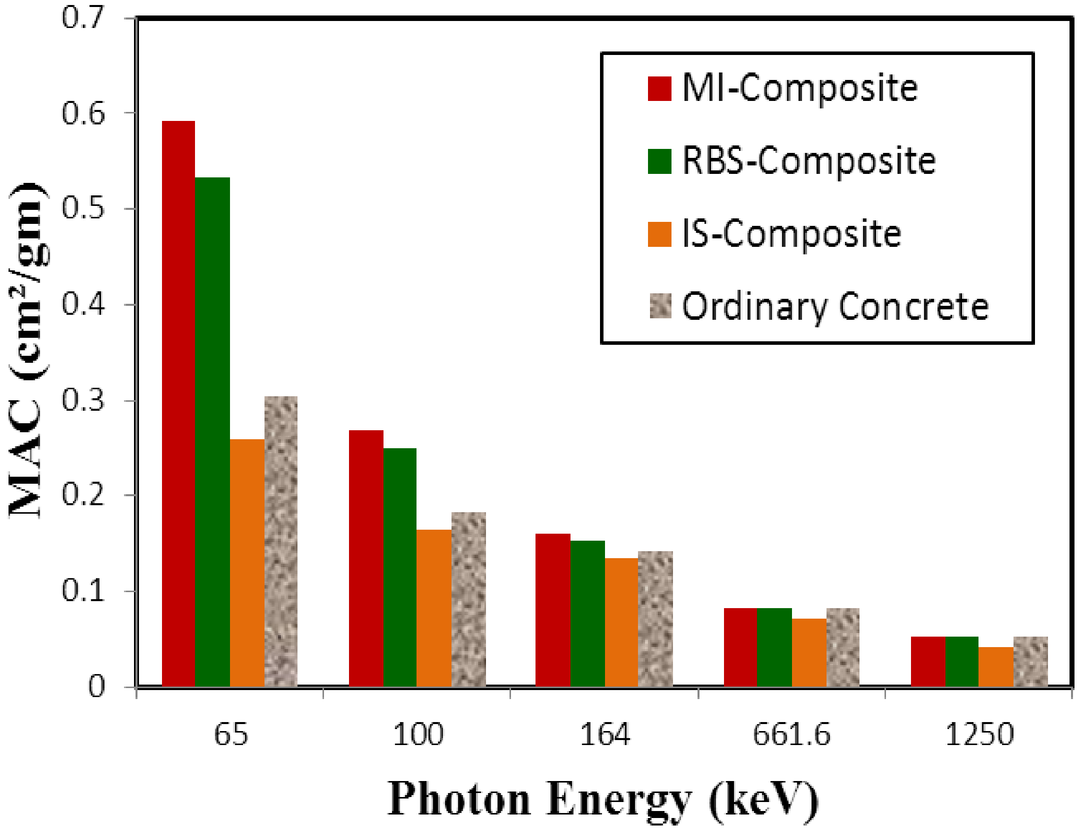

Figure-3.2: Photon Energy (keV) Vs. MAC (cm^2/gm.) (on 04.10.202)

The average of the measured mass attenuation coefficient values of similar samples (RBS) at the same energy (661.6 keV) in different countries are presented in Table-5.

Table-5: Comparison of MAC for RBS-sample in different countries

S.N	Sample	MAC (cm^2g^{-1}) for 661.6 keV	Country	References
1.	RBS-Composite	0.080	Jordan	Awadalah and Imran [36]
2.		0.078	Nigeria	Folorunso et al. [35]
3.		0.081	Bangladesh	Current work

The MAC value from Jordan agreed very well (difference only 1.23%) with the present value at the same energy level of 661.6 keV while those reported from Nigeria was slightly lower than that of the current study with a percentage difference that ranged between 3.7% and 36.76%. The samples from Nigeria would, therefore, have contained some other lighter elements that cause the density lower.

3.6 Assessment of LAC, MAC by RMI Factors

Depending on the interacting particle/field in the matter (electrons, nucleons, electric field surrounding nuclei/electrons etc.) with the mono-energetic photon of X-ray and γ-ray, the measured LAC, MAC data of the fabricated composites are assessedby RMI factors which comprisedthe complete absorption, elastic/coherent scattering or inelastic/incoherent scattering. On the basis of the probability of occurrence,the behavior of the three major RMI factors (photoelectric absorption, Compton scattering and pair production)are shown in Figure-3.3and Figure-3.4 [5]. These figures represented the graphical demonstrations of the process in which X-ray and γ-ray are attenuated.

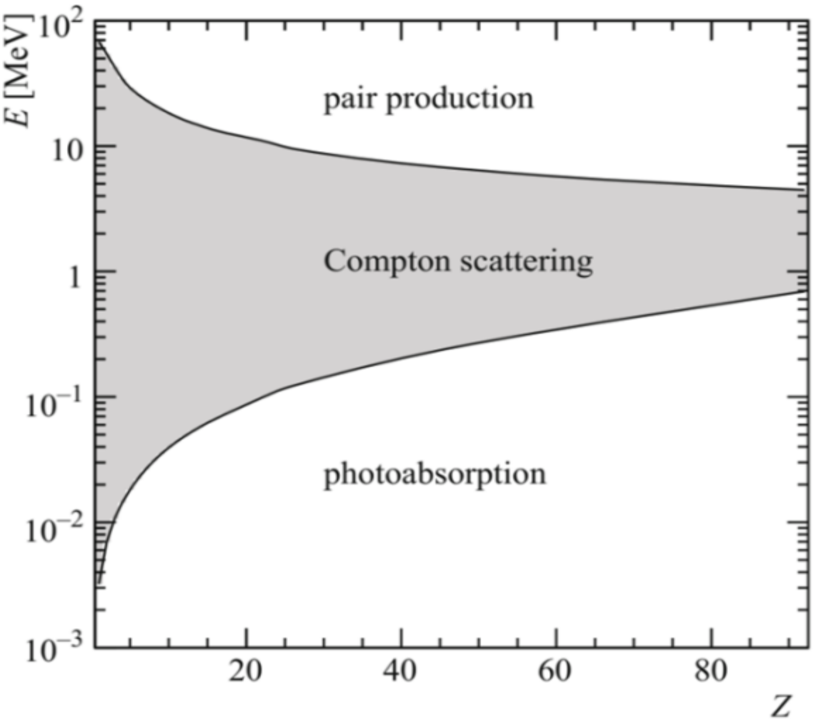

Figure-3.3: Photon Energy Vs. Atomic Number (Z)

The photon of X-ray and γ-ray interacts with the electron (mostly from K-shell) of the substance which consequences in the complete absorption of the photon. The threshold energy forthis process to happen depends upon the binding energy of the electron in a specific shell. The cross-section for photoelectric effect/absorption strongly depends on atomic number (Z) of an element. It is found that this photon interaction route is dominant for heavy elements (having high Z) at lower photon energy regions.The experimented X-ray sources have lower levels of photon energy (65 keV to 164 keV) which usually can generate the photoelectric effect RMI during the penetration of fabricated composite blocks. At this energy region, the X-ray photon can also offer few Compton scattering RMI during the penetration.

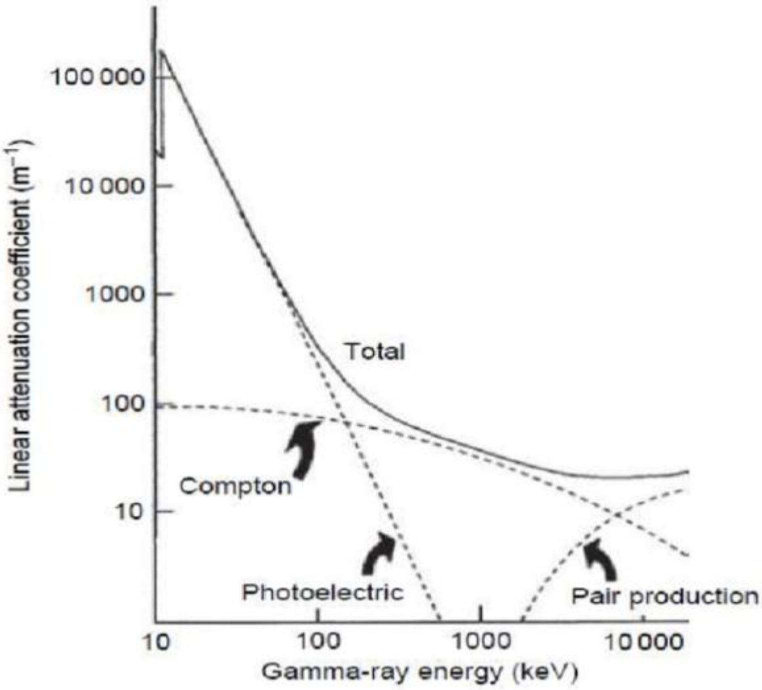

Figure-3.4: Linear Attenuation Coefficient Vs. Gamma-ray Energy

As a result of the inelastic/incoherent scattering process, partial photon energy has been transferred to an electron and the photon is scattered with the rest of the energy. Hence, this process results in only energy degradation of the gamma photon. The cross-section for the Compton scattering process is least dependent on atomic number and slowly decreases with the increase in the energy of X-ray and γ-ray. This route is dominant at the intermediate photon energy region for all elements of the composite blocks.The ^{137}Cs source has the intermediate level of γ-ray photon energy (661.6 keV) which can generate the photoelectric effect, Compton scattering RMI during the penetration of fabricated composite blocks.

At high energy, the complete absorption of γ-ray photon in the electric field of nuclei/electrons occurs, which consequences in the formation of an electron-positron pair. The threshold-value for this route to occur is 1.022 MeV (which is equivalent to the sum of rest mass of an electron and positron). For γ-photon with higher energy, the excess energy is shifted as kinetic energy to electron–positron pair. This procedure is the best example for transformation of energy into mass. The cross-section for pair production in the electric field of a nucleus differs directly with atomic number. Hence, it is a dominant process for heavy elements at higher photon energy regions [6-14]. The ^{60}Co source has high energy (average energy of 1250 keV) γ-ray photon which can create thephotoelectric effect, Compton scattering as well as the pair production RMI during the penetration of fabricated composite blocks.

3.7: Electron Density Dependency

The higher the electron density, the more interaction of X-ray and γ-ray photons with the sample material occurs. These interactions can cause the absorption of the radiation photons (removal from the beam) or scattering (change of direction of beam with reduction in energy). It is clear that all the MI and RBS composites have higher and nearly the same attenuation properties in comparison to ordinary at specified X-ray and γ-ray. This is because of their higher and nearly same density values shown in (Figure-3.2). That results from the decent radiation shielding effectiveness of the material. On the other hand, due to having lower density the IS and DS composites shows very poor shielding efficiency.

3.8: Photon Energy Dependency

The photoelectric process is the predominant mode of interaction for X-rays of relatively low energy (65 keV - 164 keV);whereas at the higher energy of γ-rays at 661.6 keV and 1250 keV, the Compton scattering and pair production phenomena are dominant (figure-3.1, figure-3.2 and figure-3.3). At low energies, the LAC, MAC decrease sharply due to the dominance of photoelectric effect. The LAC, MAC values of MI and RBS composite are significantly higher than ordinary concrete at a low incident photon energy of X-ray where photoelectric absorption is the dominant interaction process.

3.9 Comparison of LAC between Madupur Clay and Brown Type Clay

Figure-3.5 & Figure-3.6 exhibit the attenuation properties in terms of LAC at various photon energy levels for Madhupur clay and Gray type clay (STC-G) based MI and

RBS composites. The Madhupur clay-based composites show slightly higher attenuation behavior than that of the Gray type clay-based composites.

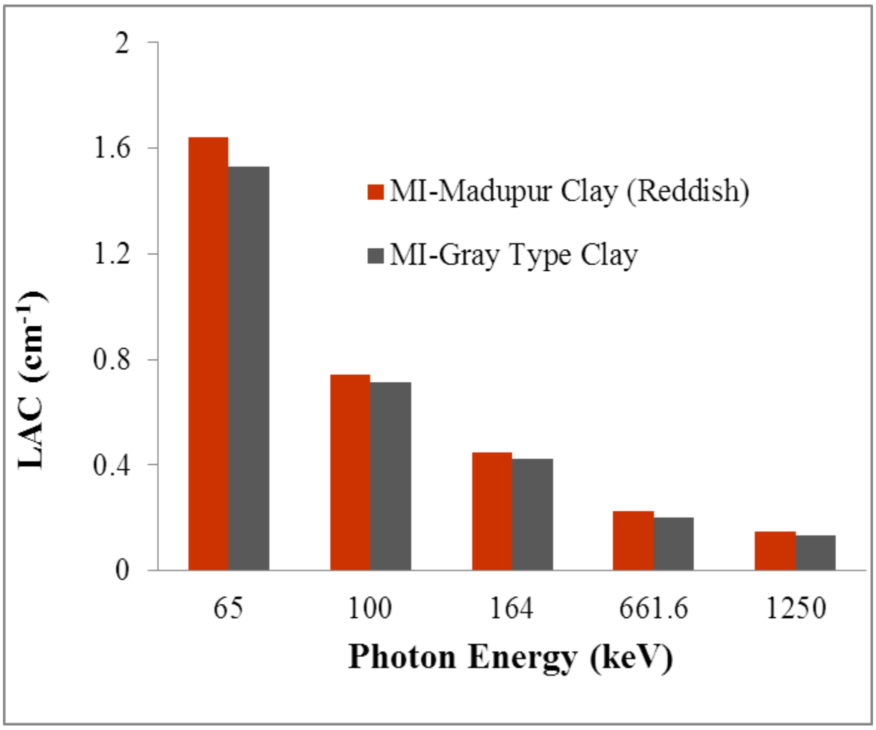

Figure-3.5: Photon Energy (keV) Vs. LAC (cm^{-1}) for Madhupur clay and Gray type clay based MI-composite on 05.11.2020.

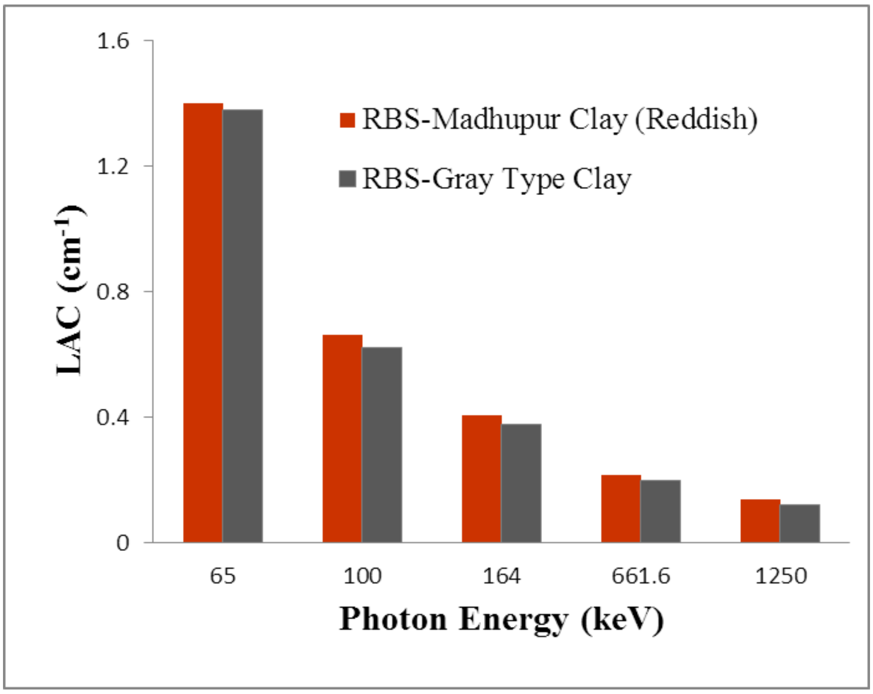

Figure-3.6: Photon Energy (keV) Vs. LAC (cm^{-1}) for Madhupur clay and Gray type clay based RBS-composite on 05.11.2020.

3.10 Half Value Layer (HVL) Evaluation

To design and choice a proper shielding material, all the nuclear-parameters associated with it needs to be considered thoroughly. HVL is an important parameter that reflects the fact that energetic photons have the competency to penetrate a sample with the raise of photon energy. The HVL was evaluated from the obtained experimental linear attenuation coefficient values [16]. The results are listed in Tables 5. From Tables 5, it can be observed that the values of HVL increase with an increase in photon energy for all the samples. It has to be noted that at each specified mono-energetic radiation, HVL values of MI and RBS composite are nearly the same and also lower than that of ordinary concrete which indicates their better efficiency of ionizing radiation shielding.

Table-6: HVL of the composites (in cm) for mono-energetic radiation photon

Photon Energy (keV)	MI-Comp.	RBS-Comp.	IS-Comp.	Ord. Con.
65	0.421	0.494	1.345	0.964
100	0.931	1.049	2.118	1.601
164	1.551	1.711	2.733	2.062
661.6	3.052	3.213	4.466	3.614
1250	4.746	5.0292	7.110	5.273

3.11 Thickness vs. LAC Evaluation

The variation of the experimental LAC values is primarily due to their dependence on the particular thickness of the samples. Figure-3.7 &Figure-3.8 demonstrate the competence of the fabricated shielding blocks with respect to the ordinary concrete for both Cs-137 and Co-60 sources.The figure-3.7 illustrates the significant differences in the necessity of shielding thickness. The LAC values increases as the thickness increases. At the lower thickness region, the LAC values were increased slowly, while at the high thickness region (more than 3.6 cm), the LAC values were elevated remarkably, especially for MI-composite and RBS-composite.

The figure-3.8 also expresses the shielding effectiveness of beach sand and heavy mineral containing composite blocks at various thicknesses with respect to ordinary concrete.It was also detected that the raw beach sand and mineral based composites have a much better result with respect to ordinary concrete even at the lower level of thickness for both radiation emitting sources. The IS-composite exhibits very poor attenuation capacities at various thickness levels.

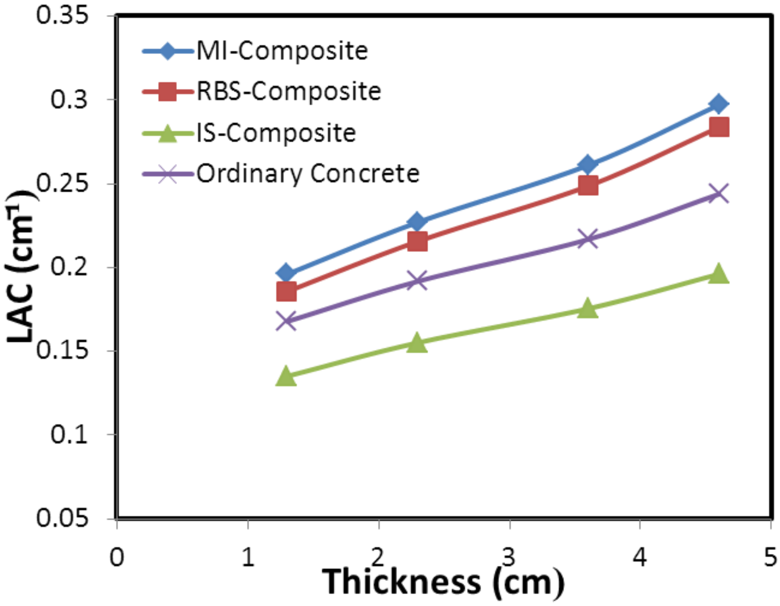

Figure-3.7: Thickness Vs. LAC (cm^{-1}); Source: Cs-137 (661.6 keV)

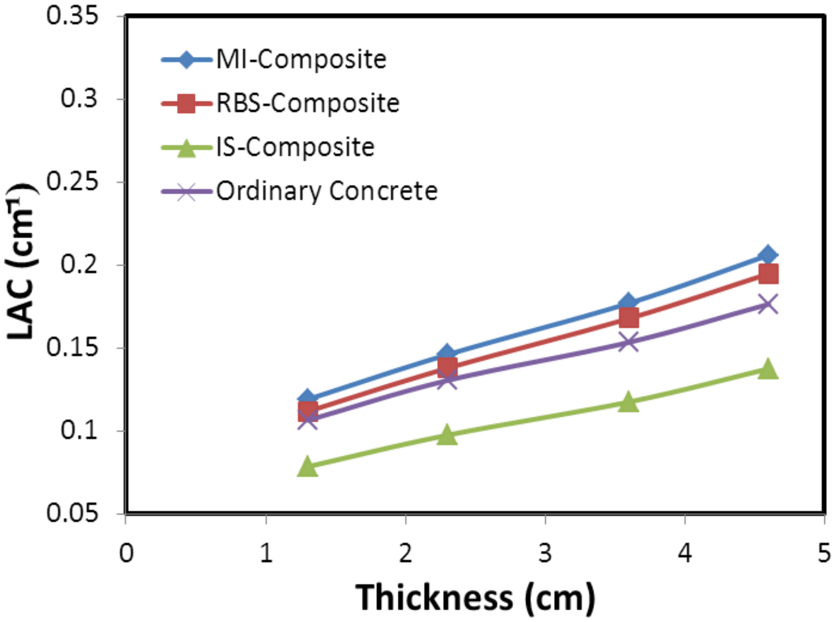

Figure-3.8: Thickness Vs. LAC (cm^{-1});Source: Co-60 (1250 keV)

As the HVL shielding factor is related to the thickness of the shielding block, the thinner composite block will play a vital role to design and fabricate an optimized shielding material.

3.12 Effect of Bi-Oxide as Additive

Beside matrix and filler of the composites, the effect of the bismuth oxide (Bi_2O_3) as additive on LAC for various mono-energetic photons was evaluated.Figure-3.9 represents the comparison of LAC values for RBS, Bi-RBS composites and ordinary concrete.

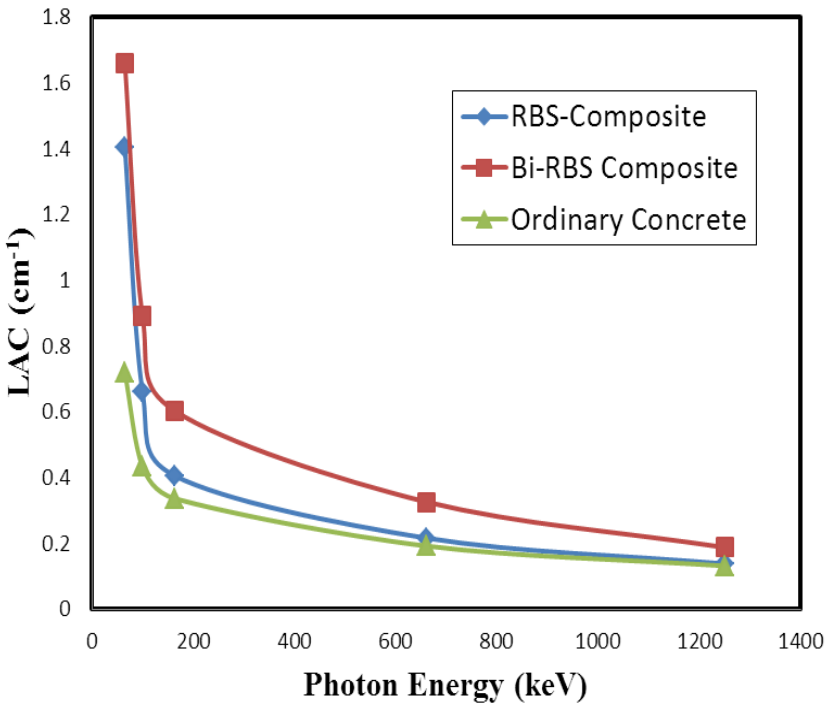

Figure-3.9: Effect of bismuth oxide as additive on LAC for various photon energies.

The Bi-RBS composite exhibits a very high level of attenuation behavior with respect to RBS composite and ordinary concrete [15]. Due to the high specific gravity of bismuth, the bismuth oxide incorporated Bi-RBS composite can cause more interaction with the incident photon which results in more attenuation. But due to the high cost of bismuth oxide, it would not be implacable with respect to available conventional materials.

3.13 Biological Hazard Assessment

The effective dose is the tissue-weighted sum of the equivalent doses in all specified tissues and organs of the human body and represents the stochastic health risk to the whole body, which is the probability of cancer induction and genetic effects, of low levels of ionizing radiation [16-18]. The Figure-3.10 shows the effective dose rates (EDR) of the hazardous ionizing radiations at various photon energies for the fabricated composites.

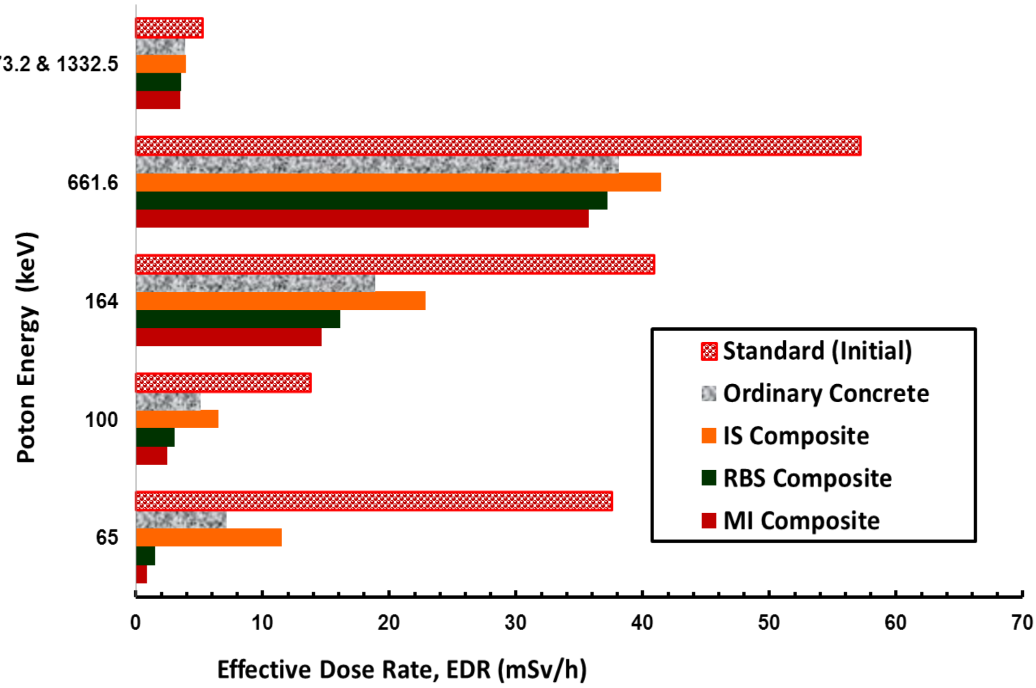

Figure-3.10: Effective Dose Rates of the composites on 18.11.2020.

The used X-ray sources were (65, 100 and 164 keV) and γ-ray sources were: Cs-137 (661.5 keV) of 20 Ci and Co-60 (1173.2 & 1332.5 keV): 1 Ci. For each photon energy level, the MI and RBS composites have superior efficiency in biological shielding compared to ordinary concrete due to their effective dose rates minimizing capability. The IS composite exhibits inferior capability in biological hazard minimizing events. At an energy level of 661.6 keV (20 Ci), the EDR values are higher. Because; the 20 Ci Cs-137 is high enough to create the high initial value of EDR. But at low photon energy level, the EDR values of MI & RBS composites drop drastically, which reveals the minimum exposure to the object and mitigates the health risk.

3.14 Elemental Analysis by NAA

The key elemental composition & abundance of Magnetite (Mag.), Ilmenite (Ilm.), Raw Beach Sand (RBS), Inland Sand (IS), cement and clay have been determined by the neutron activation analysis (NAA) technique using 3MW TRIGA Mark-II research reactor at Savar, Dhaka, Bangladesh. The measured key elemental abundance (Na, Al, K, Sc, Ti, V, Cr, Mn, Fe, Co, Zn, As, Rb, Sb, Ba, La, Ce, Sm, Eu, Dy, Yb, Lu, Hf, Ta, Th and U) and the literature value of Upper of Continental Crust (UCC; Rudnick, Elsevier-2014) were tabulated in Table-7 .

Table-7: The key elemental composition & abundance of Magnetite (Mag.), Ilmenite (Ilm.), Raw Beach Sand (RBS), Inland Sand (IS), Cement, Clay and the literature data of UCC.

Elements	Unit	Specific Gravity	Magnetite	±	Ilmenite	±	RBS	±	IS	±	Cement	±	Clay	±	UCC.
Na	%	0.96	0.012	0.00	0.019	0.001	0.041	0.001	1.153	0.013	0.072	0.001	0.337	0.002	3.27
Al	%	2.7	0.356	0.01	0.371	0.006	3.101	0.028	5.597	0.039	4.684	0.038	5.97	0.04	15.4
K	%	0.86	0.028	0.00	0.081	0.009	1.528	0.037	1.893	0.043	0.437	0.095	1.11	0.03	2.8
Sc	µg/g	2.98	5.37	0.05	37.20	0.300	41.053	0.119	7.294	0.030	11.99	0.056	10.37	0.09	14
Ti	%	4.5	1.277	0.06	25.21	0.946	6.933	0.270	0.259	0.021	0.257	0.021	0.497	0.029	0.64
V	µg/g	6	1510	0.00	0.113	20.00	723.556	14.061	52.65	2.390	68.42	2.864	182	5	97
Cr	µg/g	7.19	3040	60.0	2510	0.004	2312.502	21.187	45.64	0.650	59.60	1.032	83	2	92
Mn	µg/g	7.21	2170	110.0	8190	180.0	5972.945	71.186	385.9	5.625	988.03	213.6	339	19	1000
Fe	%	7.87	70.23	0.36	41.47	0.253	41.907	0.314	2.15	0.023	2.273	0.031	2.3	0.04	5.04
Co	µg/g	8.9	48.5	0.00	0.004	0.000	32.905	0.435	5.609	0.115	7.300	0.184	9.02	0.38	17.3
Zn	µg/g	7.14	290	20.0	220.0	20.0	310.196	7.993	28.48	1.155	35.887	1.804	BDL	BDL	67

U	Th	Ta	Hf	Lu	Yb	Dy	Eu	Sm	Ce	La	Ba	Sb	Rb	As
µg/g	µg/g	µg/g	µg/g	µg/g	µg/g	µg/g	µg/g	µg/g	µg/g	µg/g	µg/g	µg/g	µg/g	µg/g
19.1	11.7	16.6	13.3	9.84	6.9	8.54	5.26	7.52	4.4	6.16	3.51	6.7	1.5	5.72
2.17	8.5	0.92	6.4	0.19	2.2	2.93	0.78	2.75	29.8	11.5	420	<0.08	<3.8	4.2
0.09	0.20	0.04	0.20	0.01	0.10	0.08	0.03	0.03	0.30	0.30	20.0	BDL	BDL	0.20
7.8	24.8	32.6	16.2	0.88	13.1	7.8	1.28	7.61	73.2	32.5	326	1.17	<3.8	2.90
0.40	0.50	0.80	0.30	0.03	0.40	0.70	0.05	0.04	0.90	0.6	19.0	0.09	BDL	0.20
129.22	991.09	64.85	617.157	11.37	69.109	88.466	13.266	221.374	2831.523	1527.991	768.649	0.384	107.457	2.452
1.74	5.874	2.722	8.797	0.130	0.927	0.717	0.373	0.416	17.609	7.311	17.576	0.017	2.548	0.072
2.75	14.82	0.578	6.459	0.58	3.393	6.778	1.331	8.410	118.3	64.26	313.4	0.118	82.56	1.574
0.083	0.111	0.032	0.105	0.011	0.113	0.110	0.048	0.032	0.899	0.539	9.363	0.009	2.175	0.058
4.36	9.863	0.528	3.572	0.53	6.137	4.557	1.410	6.071	70.76	37.882	305.75	1.185	31.483	10.637
0.108	0.103	0.038	0.078	0.016	0.240	0.085	0.062	0.026	0.759	0.378	12.33	0.030	1.466	0.150
5.32	24.2	1.7	15.3	0.811	4.88	7.5	1.81	10.26	77.9	59.6	387	0.522	96	3.4
0.15	0.3	0.12	0.2	0.026	0.17	0.3	0.13	0.04	0.9	0.6	13	0.025	5	0.1
2.7	10.5	0.9	5.3	0.31	2	3.9	1	4.7	63	31	625	0.4	84	4.8

Note: Elem.: Element, Sp.G: Specific Gravity, BDL= Below Detection Limit.

It is identified that elemental contents are widely varied in different types of sample ingredients. The precious heavy sand mineral (Magnetite, Ilmenite) were separated based on the specific gravity, particle size, electrical conductivity and magnetic susceptibility. The Table-7: shows that Magnetite contains the highest abundance of Fe (70.23%). The Ilmenite also has higher amount of Fe (41.47%) & Ti (25.21%), which results in more dense composites. The Magnetite and Ilmenite minerals are the main source of iron (Fe) in the raw beach sands. In order to make a general graphical comparison, Normalized values (Measured value ÷ Maximum value) of the elemental abundance were shown in figure-3.11.

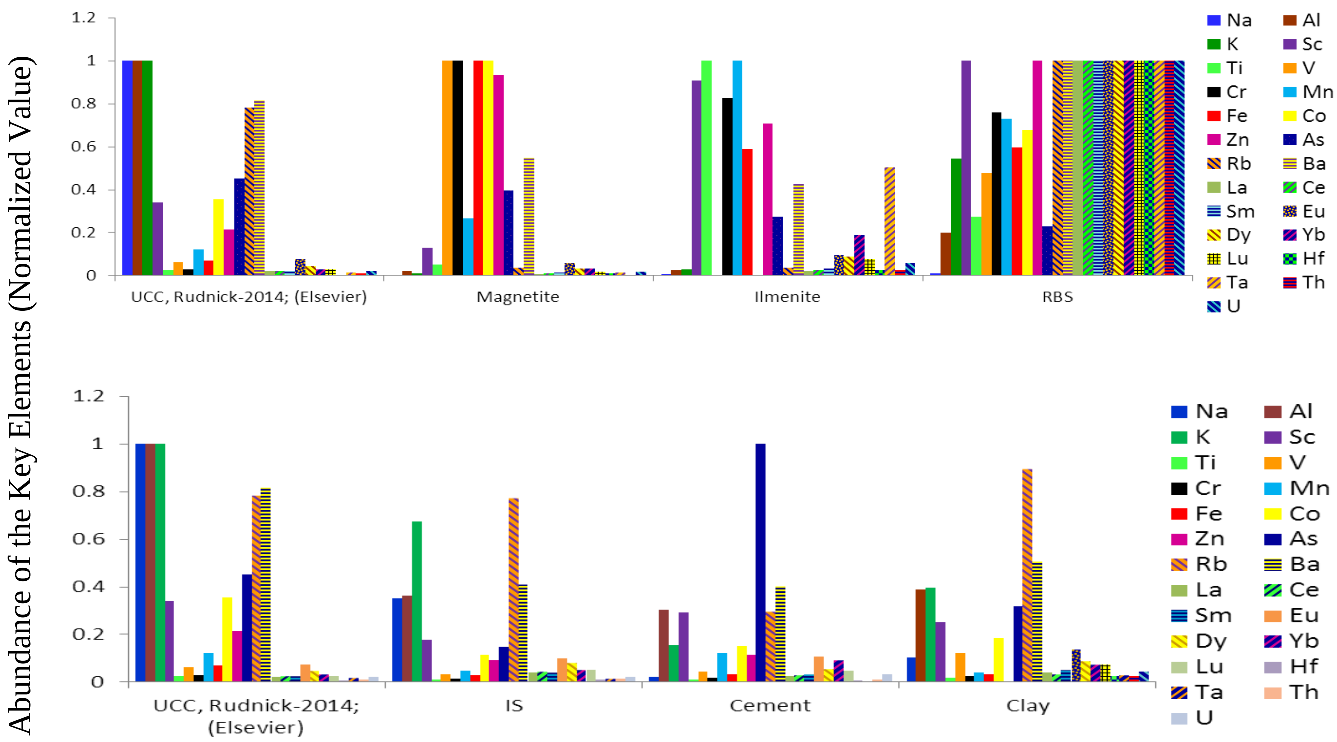

Figure-3.11: Normalized value of the elemental abundance for the key elements.

The NAA study reveals that magnetite and Ilmenite have a significantly large amount of Fe and Ti elements. This study also represents that the inland sand(IS) contains a low abundance of heavy elements than those raw beach sand (RBS). On the other hand, the raw beach sand containsa significantly high level of heavy elements (Sc, Ti, V, Cr, Mn, Fe, Co, Zn, Rb, Ba, rare earth metals and Th, U) and low level of light elements (Na, Al, K etc.) with respect to the reference (UCC) and IS, which are mainly responsible for high density of the material. As the binder (matrix) ingredient, clay and cement have been used to fabricate the composite blocks. Among these two ingredients, cement has a significantly higher amount of arsenic (10.63µg/g) and antimony (1.18µg/g).The Madhupur clay has a relatively higher amount of trace elements (heavy metals like, Rb, Sb, La, Ce, Sm, Eu, Dy, Yb, Lu, Hf, Ta, Th, U) with respect to the upper continental crust of CCC literature value [19-22].

3.15 Heavy Elemental Concentration Impact on Photon Attenuation Properties

The NAA elemental analysis reveals that the separated beach minerals (magnetite and Ilmenite) contain a very high level of Fe & Ti concentration and the raw beach sand of Cox's Bazar contains a significantly high level of heavy element concentration. Therefore, the MI and RBS composites exhibit high density (eventually, greater than ordinary concrete). When these heavy elements containing MI and RBS composites are exposed by the mono-energetic photon of X-ray and γ-ray, the huge number of interactions (photoelectric absorption, Compton effect, pair production etc.) occur. That results in the weakening of the photon energy and uplifting the attenuation properties. Conversely, having a lower level of heavy elements, the IS composite shows very poor density. Hence, the number of interactions becomes low and the ionizing radiations can penetrate easily.

3.16 Morphology Study of the Composites by NR

Neutron radiography (NR) has been performed to study the internal structural and morphological characterization of the composites using the thermal neutron at TRIGA Mark-II reactor. Using the NR method the whole internal morphology study was done due to the high penetration behavior of chargeless neutron. The neutron radiographic image represents the attenuating behavior of the thermal neutron beam due to the constituents within the composites.

As the thermal neutron can penetrate easily through the composite blocks, it hits the Gd-foil converter and e^--particle is generated following the $^{157}Gd\,(n, e^-)\,^{158}Gd$ nuclear reaction. The produced e^- particle is then exposed to the photographic film, which produces a bright signal. On the other hand, attenuation of thermal neutron beam is mainly due to scattering and absorption of neutrons. The high density composite material can scatter and absorb the thermal neutron which results in low exposure of e^- particles to the photographic film, which produces a deep dark signal. The figure-3.12 – figure-3.15 exhibits the morphological investigation of the composite materials by neutron imaging (neutron radiography).

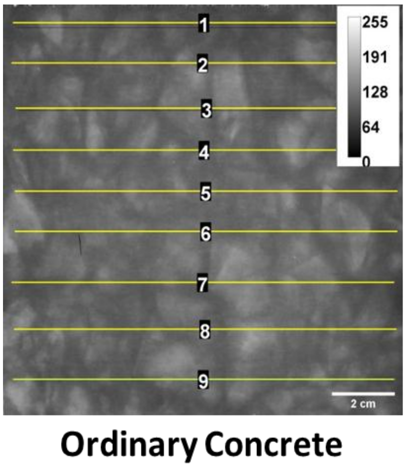

Figure-3.12: Neutron imaging of the ordinary concrete (NR morphology study)

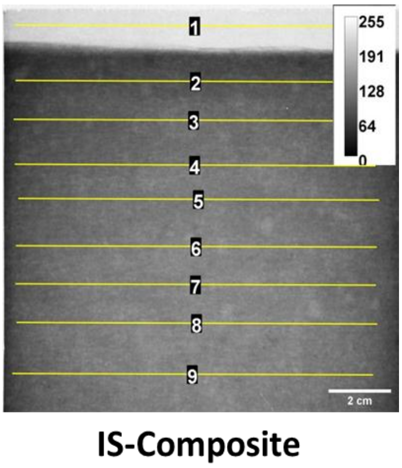

Figure-3.13: Neutron imaging of the IS composite (NR morphology study)

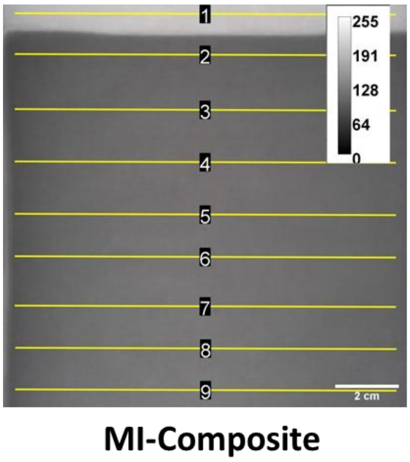

Figure-3.14: Neutron imaging of the MI composite (NR morphology study)

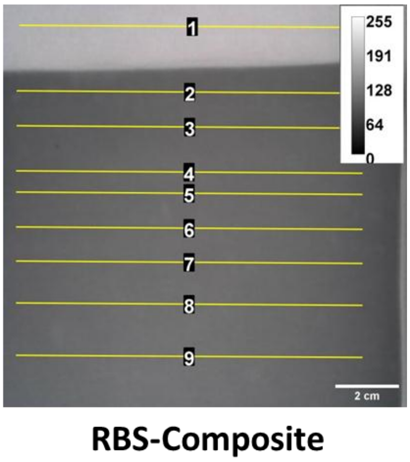

Figure-3.15: Neutron imaging of the RBS composite (NR morphology study)

The MI & RBS composites show deep dark and uniform signals in neutron image that indicates their higher level of attenuation behavior. In contrast with that, ordinary concrete has a mixture of deep dark and bright neutron images with heterogeneous morphological structures. The bright parts indicate easy penetration of thermal neutron. Though ordinary concrete has some brighter parts in the neutron image, the chemical bonding of the cementingingredient makes the composite moderate attenuation. The IS composite shows a comparatively lower dark image than those of MI & RBS composites, which causes its lowest attenuation behavior among the studied composite materials [23-24].

3.17 Illustration of Neutron Images of the Composites by Image J software

In order to illustrate the neutron image of the composites, Image J software was implemented, which was explained by gray value and pixel for various regions of interest (ROI). The gray value indicates the degree of brightness at various pixels. As the gray value increases, the brightness increases which results in the lower attenuation of the composite. The gray values of the composites at various pixel points were shown in the figure-3.16.

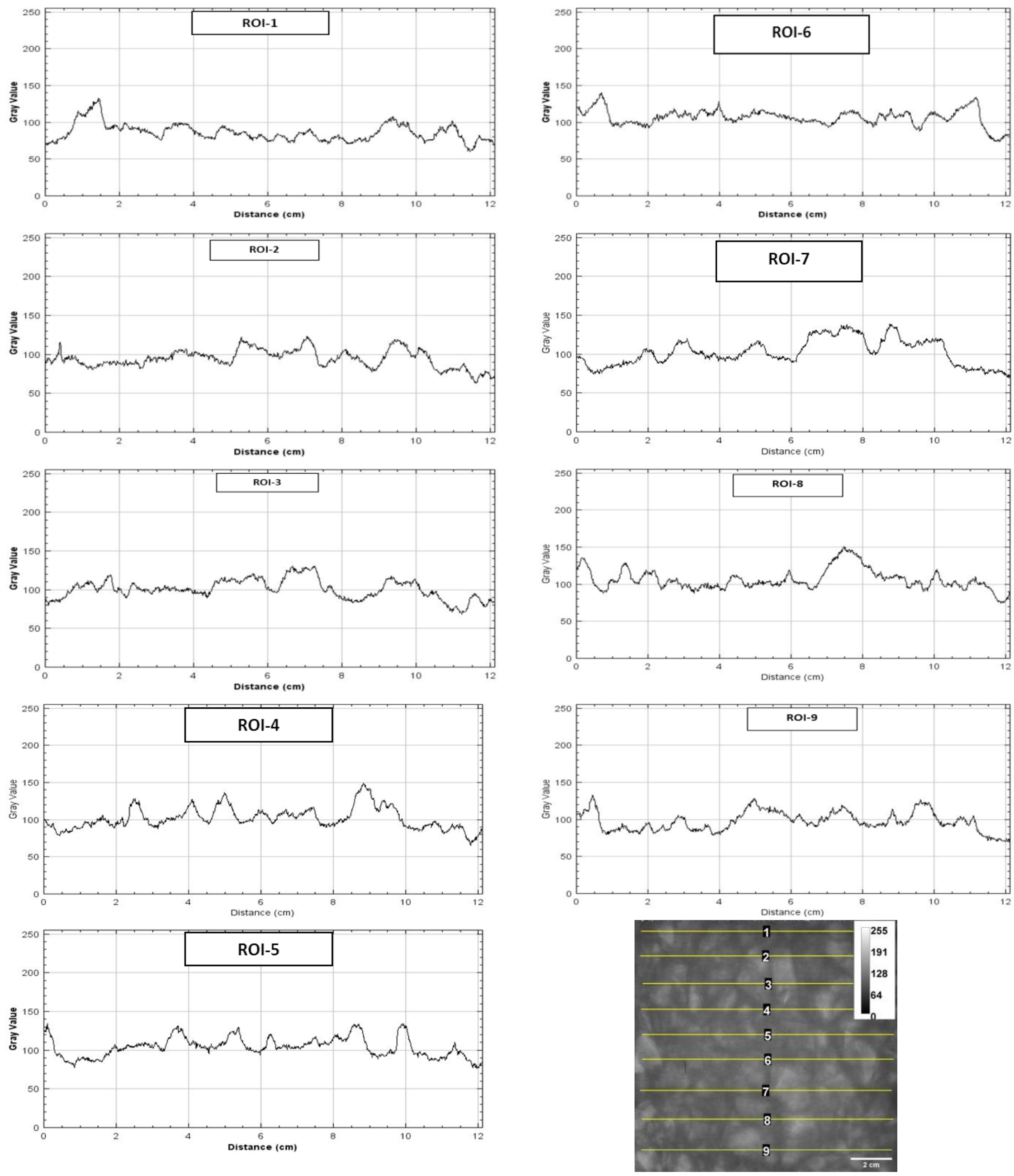

Figure-3.16: The gray value curves at different pixels (distance) for various ROIs of ordinary concrete

In Figure-3.16, the ordinary concrete shows the fluctuating curves of gray values at various ROIs (ROI-1 to ROI-9). The fluctuation curves of gray values for pixel (distance) confirm the heterogeneous morphology of the ordinary concrete.

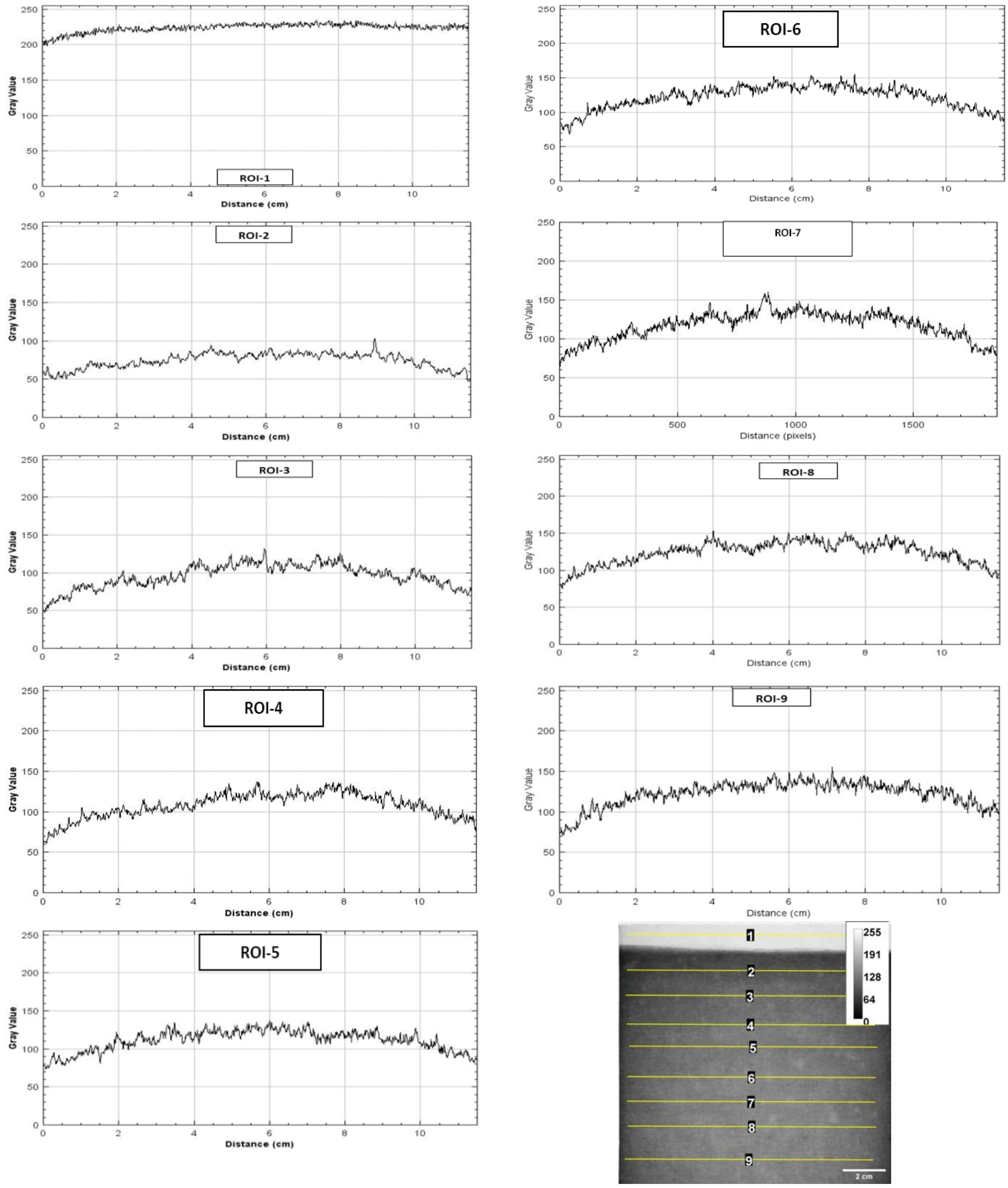

Figure-3.17: The gray value curves at different pixels (distance) for various ROIs of IS composite

In Figure-3.17, the IS composite shows the almost steady curves of gray values at various ROIs (ROI-1 to ROI-9). The almost steady curves of gray values for pixel (distance) indicate the nearly homogeneous morphology of the IS composite.

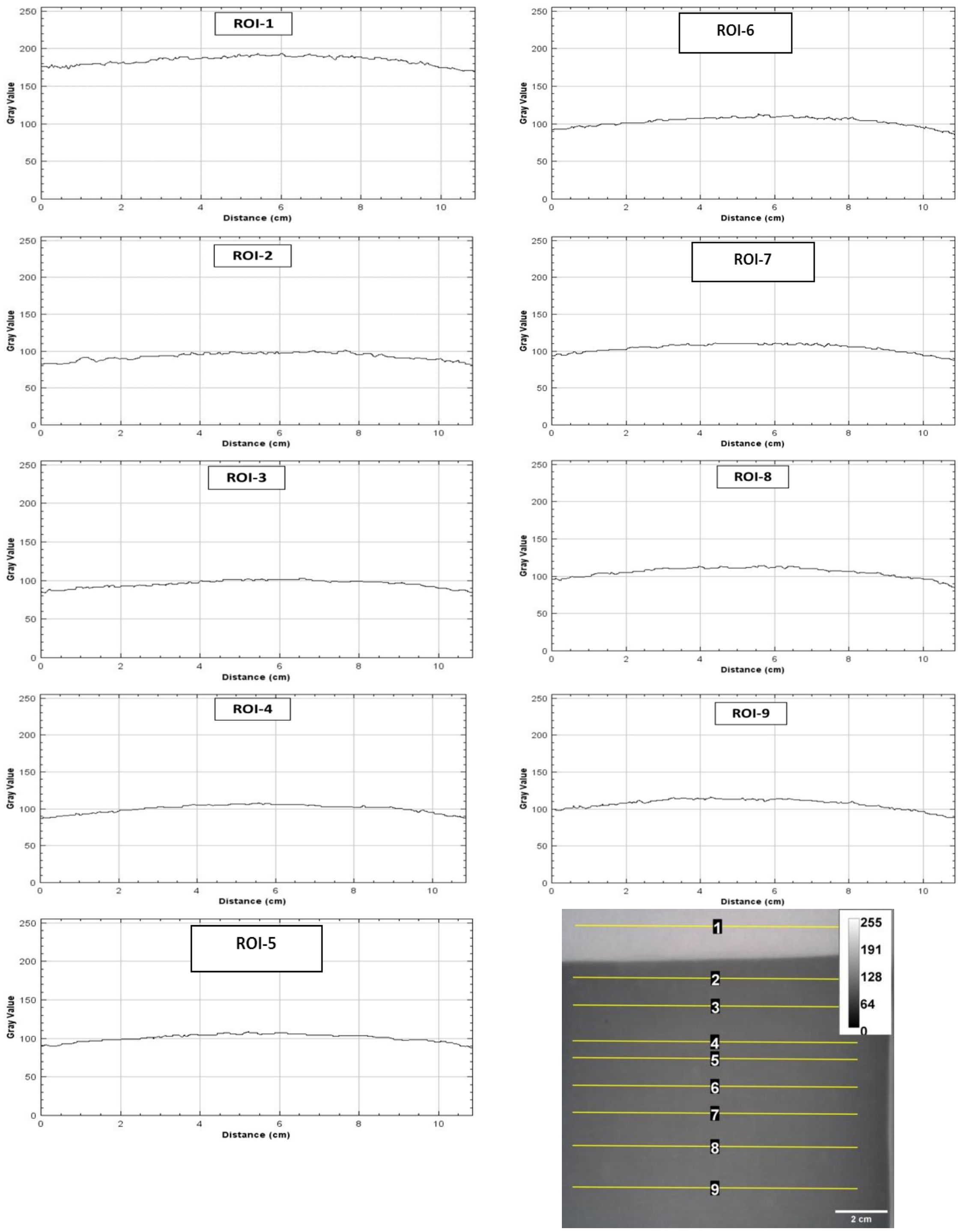

Figure-3.18: The gray value curves at different pixels (distance) for various ROI of RBS composite

In figure-3.18, the RBS composite shows the steady curves of gray values at various ROIs (ROI-1 to ROI-9). The steady curves of gray values for pixel (distance) confirm the homogeneous morphology and fine grained structure of the RBS composite.

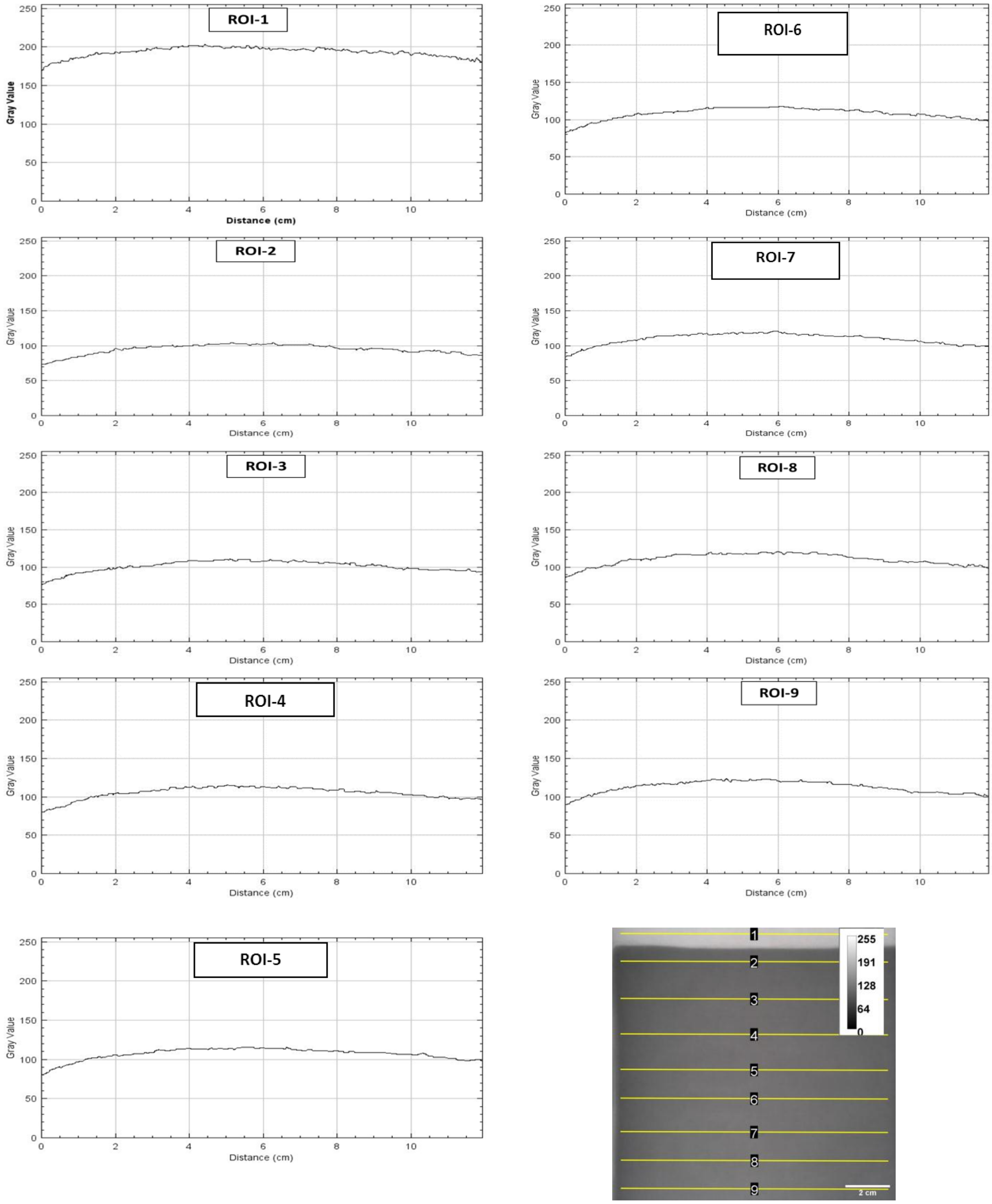

Figure-3.19: The gray value curves at different pixels (distance) for various ROIs of MI composite

In figure-3.19, the MI composite shows excellent steady curves of gray values at various ROIs (ROI-1 to ROI-9). The steady curves of gray values for pixel (distance) confirm the homogeneous morphology and fine grained structure of the MI composite. The morphology study reveals that the internal finely structured clay based MI & RBS composites have steady gray values than that of ordinary concretes, which indicates the lower transmission and higher attenuation of the ionizing radiation (X-ray, γ-ray etc.). Therefore, the NR study has a good agreement with the shielding factors (LAC, MAC, HVL etc.) of the studied composites.

3.18 Mechanical Properties Analysis

The ordinary concrete shows better mechanical properties than the fabricated clay based (MI, RBS, IS) composite blocks (Table-8). But finely grained and manual compactions make good mechanical properties of the MI & RBS composite blocks. Stress at peak indicates the tensile strength of the samples. The Stress at peak vales of ordinary concrete, MI composite, RBS composite, IS composite were 0.244 N/mm^2, 0.086 N/mm^2, 0.081 N/mm^2, 0.072 n/mm^2 respectively.

Table-8: Mechanical properties of the fabricated composite blocks.

Sample ID	Width (mm)	Length (mm)	Thick -ness (mm)	Force @peak (N)	Elongation @Break (mm)	Stress @Peak (N/mm2)	Elongation @Peak (mm)	Stress @Break (N/mm2)	Strain @Peak (%)	Young Modulus (Mpa)
Ordinary Concrete	38.97	100	6	57	2.329	0.244	0.055	0.21	0.041	89.641
MI-Com.	38.97	100	6	20	2.504	0.086	0.083	0.043	0.062	78.855
RBS-Com.	38.97	100	6	19	2.463	0.075	0.081	0.042	0.0602	76.634
IS-Comp.	38.97	100	6	17	2.114	0.063	0.072	0.037	0.0516	72.492

3.19 Moisture Content Desorption Measurement

The figure-3.20 exhibits the moisture content desorption rate by Gravimetric Method.

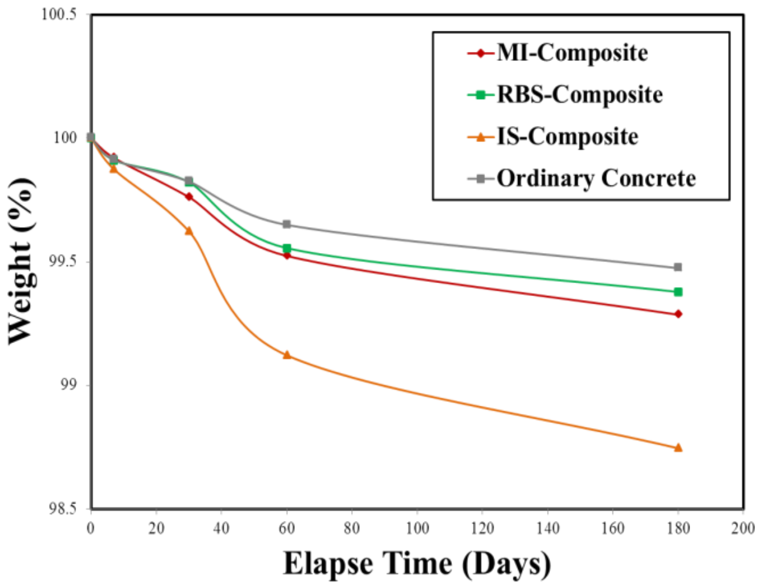

Figure-3.20: Weight (g) in elapse time (days)

At Room Temperature:

- ❖ Water desorption has occurred slowly due to the chemical bonding of ordinary concrete
- ❖ On the other hand, clay based composites (specially, IS composite) shows more desorption of water because of their physical bonding. But desorption rates are very low for MI & RBS composites (>99% weight remains up to 180 days).

References

[1] D. A. Yaseen, M. Scholz, "Textile dye wastewater characteristics and constituents of synthetic effluents: a critical review; *International Journal of Environmental Science and Technology, (link.springer.com)*" Vol.16, pp.1193–1226, 2019

[1] A. S. M. Shamaun Kabir, Delwar Hossain and Rashed Abdullah, "2-D Electrical Imaging in Some Geotechnical Investigation of Madhupur Clays, Bangladesh", *Journal Geological Society of India*", Vol.77, pp.73-81, 2011

[2] https://en.banglapedia.org/index.php/Madhupur_Clay (Date: 12.03.2019, at 10.30 am)

[4] Lothenbach, Barbara, Scrivener, Karen, Hooton, R. D., "Supplementary cementitious materials", *Cement and Concrete Research*. Vol. 41 (12), pp. 1244–1256, December 2011

[5] G. Gilmore, “Ch 2 - Interactions of Gamma Radiation with Matter” *Practical Gamma-Ray Spectrometry*, Vol. 2 (2nd Edition), p. 26, 2008 (DOI:10.1002/9780470861981)

[6] F. Salvat, “PENELOPE-2014: A Code System for Monte Carlo Simulation of Electron and Photon Transport Book”, *NEA Data Bank*, Barcelona, Spain, 2015.

[7] Christian W. Fabjan; “Herwig Schopper Editors Particle Physics Reference Library, Detectors for Particles and Radiation”; *Springer*, Volume 2, 2020

[8] Michael W. Engher, Arthur Shanks, J. Sandia, “FRMAC Gamma Spectroscopist Knowledge Guide”, *National Laboratories Albuquerque, New Mexico* 87185 and Livermore, California 94550; 2019.

[9] R. Meckbach, P. Jacob, “Gamma exposures due to radionuclides deposited in urban environments. Part II: Location factors for different deposition patterns”,*Radiat. Prot. Dosim*. Vol. 25 (3), pp.181–190, 1988.

[10] R. Meckbach, I. K. BailiffGo, Y. Jacob, P.D. Stoneham, “Calculation and measurement of depth dose distributions in bricks”,*Radiat. Prot. Dosim*.,Vol. 66 (1–4), pp. 183–186, 1996.

[11] M. J. Yaffe, G. E. Mawdsley, L. Martin, R. Servant, and R. George, “Composite materials for X-ray protection,” Health Phys. Vol. 60, pp. 661–664, 1991.

[12] E. W. Webster, “Addendum to ‘Composite materials for X-ray protection’,” *Health Phys*. 61, 917–918, 1991.

[13] Cunningham J.R. and Johns H.E., “Calculation of the average energy absorbed in photon interactions”, *Med. Phys*, Vol. 7, pp. 51, 1980.

[14] R. Poggiani, “High Energy Astrophysical Techniques, UNITEXT for Physics”, *Springer International Publishing Switzerland, Chapter-2: Radiation Matter Interactions*, pp.21-23, 2017

[15] Mridula Dogra, K.J. Singh, Kulwinder Kaur, Vikas Anand, Parminder Kaur, "Gamma Ray Shielding and Structural Properties of Bi2O3-B2O3-Na2WO4 Glass System" *Universal Journal of Physics and Application*, Vol.11(5): pp.190-195, 2017

[16] P. Jacob, R. Meckbach, "Shielding factors and external dose evaluation",*Radiat. Prot. Dosim.*,Vol. 21 (1/3), pp. 79–85, 1987.

[17] G. A. Carlsson, "Absorbed Dose Equations. On the Derivation of a General Absorbed Dose Equation and Equations Valid for Different Kinds of Radiation Equilibrium", *Radiation research*, 85, 219-237 (1981)

[18] ICRP - International Commission on Radiological Protection, Recommendations of the ICRP, *ICRP Publication 103, Annals of the ICRP*, 103: pp.1-7, 2007

[19] R. L. Rudnick, S. Gao, "Composition of the continental crust", *Treatise on Geochemistry, Elsevier Ltd.*, Oxford, UK, 2nd ed., Chapter 4, pp. 1–64. (2014).

[20] A. El-Taher, "Rare earth elements content in geological samples from eastern desert, Egypt, determined by instrumental neutron activation analysis", *Appl. Radiat. Isot.* Vol. 68, pp. 1859, 2010.

[21] R. Khan, N. Shirai, M. Ebihara, "Chemical characteristic of R chondrites in the light of P, REEs, Th and U abundances", *Earth Planet. Sci. Lett.* Vol.18,422, 2015

[22] Folorunso O. Ogundare, "Low-energy broad-beam photon shielding data for constituents of concrete"; Journal oF Applied Clinical Medical Physics, Vol. 13 (Number 2), pp. 176-182, 2012

[23] M. I. Awadallah, M. M. A.Imran. "Experimental investigation of gamma-ray attenuation in Jordanian building materials using HPGe-spectrometer", *J Environ Radioact.*;Vol.94(3): pp.129–36. 2007

[24] Schneider CA, Rasband WS, Eliceiri KW. "NIH Image to ImageJ: 25 years of image analysis". *Nat Methods.* 9 (7): 671–675, 2012

CHAPTER 4

4. CONCLUSIONS

4.1 Conclusions

The indigenous ingredient-based ionizing radiation (X-ray and γ-ray of ^{60}Co & ^{137}Cs) attenuating composite shielding materials were fabricated. The effect of the additive by implementing bismuth oxide was also evaluated which is efficient but costly for radiation shielding. The experimental data revealed adequate attenuation properties compared with other conventionally used shielding materials. The present investigation shows that the Madhupur clay-based heavy mineral (magnetite, Ilmenite) and raw beach sand reinforced composite materials exhibited significantly higher radiation (both for X-ray and γ-ray) shielding capability in comparison to the ordinary concrete block, especially, for low energy diagnostic range X-ray. The inland sand-containing composite has shown a poor radiation attenuation property among the studied composites. The linear and mass attenuation coefficient (LAC, MAC) depends on the material density, sample composition and photon energy. The Magnetite-Ilmenite and Raw Beach Sand composites are outstanding, economical and less space-consuming shielding-material against hazardous ionizing radiation of X-ray and γ-ray at the mono-energetic photon energy range of 65 keV – 1250 keV. The current experimental observations would be useful for designing potential radiation shielding materials for facilitiesbased on the indigenous cost-effective raw materials. It can be applied as a biological shield for upcoming Rooppur NPP, research reactor installations, radioactive waste management facilities, accelerator facilities, X-ray installation and commercial γ-ray irradiation facilities.

4.2 Future Aspects of this Research

Shifting in radiation type (neutron-ray etc.), photon energy, layer-wise synthesis, Nano-synthesis and chemical composition would impact greatly in attenuation behavior. Metal slag, cost-effective high density additives could also be good option. The attenuation & elemental compositional data and neutron images of the studied local shielding materials would be used to choose the proper ingredients necessary for designing and constructing radiation shielding materials.